The underlying structures of self-attention: symmetry, directionality, and emergent dynamics in Transformer training

Matteo Saponati[1,*], Pascal Sager[1,2,*], Pau Vilimelis Aceituno[1],
Thilo Stadelmann[1,2,3], and Benjamin Grewe[1,4]

[1]Institute of Neuroinformatics, ETH Zürich and University of Zürich, Zürich, Switzerland
[2]Centre for Artificial Intelligence, Zürich University of Applied Sciences, Winterthur, Switzerland
[3]ECLT European Centre for Living Technology, Venice, Italy
[4]ETH AI Center, Zürich, Switzerland
[*]equal contribution

Abstract

Self-attention is essential to Transformer architectures, yet how information is embedded in the self-attention matrices and how different objective functions impact this process remains unclear. We present a mathematical framework to analyze self-attention matrices by deriving the structures governing their weight updates. Using this framework, we demonstrate that bidirectional training induces symmetry in the weight matrices, while autoregressive training results in directionality and column dominance. Our theoretical findings are validated across multiple Transformer models — including ModernBERT, GPT, LLaMA3, and Mistral — and input modalities like text, vision, and audio. Finally, we apply these insights by showing that symmetric initialization improves the performance of encoder-only models on language tasks. This mathematical analysis offers a novel theoretical perspective on how information is embedded through self-attention, thereby improving the interpretability of Transformer models.

1. Introduction

Transformer models now achieve state-of-the-art performance across a wide range of tasks and domains [Radford et al., 2019, Dosovitskiy et al., 2021, Radford et al., 2023]. Despite their success, the internal mechanisms governing their decision-making processes remain poorly understood, raising concerns regarding model alignment, reliability, and safety [Wang et al., 2023, Yao et al., 2024]. A key

challenge in understanding these models is unraveling the structures of self-attention, which is essential to Transformer architectures. Current literature largely overlooks the nature of the self-attention weight matrices during autoregressive training, where the model predicts the next token in a sequence given previous ones [Radford et al., 2019, Black et al., 2021, Touvron et al., 2023] and bidirectional training, where the model predicts a missing token given the full sequence [Devlin et al., 2019, Bao et al., 2022, Warner et al., 2024]. Understanding self-attention requires answering two fundamental questions: How can we interpret the structures learned in the self-attention matrices? What is the impact of different objective functions on these matrices?

Previous work used sparse auto-encoders to identify interpretable features [Huben et al., 2024, Bricken et al., 2023], circuit analysis to interpret Transformer components [Olah et al., 2020, Elhage et al., 2021, Olah, 2022], and techniques like the logit lens to analyze self-attention mechanisms [Geva et al., 2021, Dar et al., 2023] (for a detailed discussion, see Section 5). However, these methods do not reveal the structural patterns in self-attention matrices or the transformations they encode. Crucially, how autoregressive and bidirectional training shape specific weight structures remains unclear.

To address this gap, we introduce a novel framework for analyzing self-attention matrices and understanding how different objective functions define their weight updates. We then use this framework to derive understandable mathematical structures that should emerge from such updates. Finally,

---

we verify these interpretable structures numerically on many pre-trained and custom models across different modalities, supporting the universality of our results. Identifying these universal structures is fundamental not only for improving the performance of Transformer models, but also for their safety, alignment, and interpretability [Olah, 2022].

Specifically, we connect the matrix $\mathbf{W}_{qk} = \mathbf{W}_q \mathbf{W}_k^\top$ of self-attention with bilinear forms, offering novel insights compared to studying query and key matrices alone. We reveal structured patterns in the implicit weight updates of $\mathbf{W}_{qk}$, uncovering key differences between encoder-only and decoder-only models:

1. *Decoder-only models*: Training with an autoregressive objective produces a few columns with disproportionately high norms, introducing directionality in $\mathbf{W}_{qk}$.

2. *Encoder-only models*: Bidirectional optimization induces symmetric structures in $\mathbf{W}_{qk}$, reflecting the balanced nature of the training objective.

3. We validate these theoretical findings across diverse Transformer architectures and input modalities, showing that they generalize across models and tasks.

4. Empirically, we find that symmetric structures in $\mathbf{W}_{qk}$ enhance training efficiency for encoder-only models, leading to higher accuracy and faster convergence in language tasks.

2. Autoregressive and bidirectional training leads to directional and symmetric weight updates

In this section, we introduce a novel framework that links the self-attention matrices $\mathbf{W}_{qk}$ to bilinear forms, enabling us to analyze how an objective function influences their structure. This approach reveals fundamental patterns in $\mathbf{W}_{qk}$ that are not apparent when examining $\mathbf{W}_q$ and $\mathbf{W}_k$ separately. For example, we prove that autoregressive and bidirectional training induce directional and symmetric structures in the $\mathbf{W}_{qk}$ matrices. In the following sections, we define and formalize these concepts.

2.1. Interpreting self-attention with bilinear forms

Self-attention [Vaswani et al., 2017, Radford et al., 2019] is a type of score function $A : \mathbf{R}^{N,d} \times \mathbf{R}^{N,d} \rightarrow$

$\mathbf{R}^{N,N}$ that maps a sequence of N token embeddings with dimension d into a matrix of attention scores. Except for the row-wise softmax function $\sigma(\cdot)$, self-attention is a linear transformation of the embedded tokens. In particular,

$$\begin{aligned} \mathbf{A}(\mathbf{X}) &= \sigma\left(\frac{1}{\sqrt{d}} \hat{\mathbf{A}}(\mathbf{X})\right) \\ &= \sigma\left(\frac{1}{\sqrt{d}} \mathbf{Q}\mathbf{K}^T\right) \\ &= \sigma\left(\frac{1}{\sqrt{d}} \mathbf{X}\mathbf{W}_{qk}\mathbf{X}^T\right), \end{aligned} \quad (1)$$

where $\hat{\mathbf{A}}(\mathbf{X})$ is the linear part of self-attention (raw unscaled attention scores), $\mathbf{X} = [\mathbf{x}_1^\top, \ldots, \mathbf{x}_N^\top] \in \mathbb{R}^{N,d}$ is the sequence of N token embeddings $\mathbf{x}_i \in \mathbb{R}^d$, and $\mathbf{W}_{qk} = \mathbf{W}_q \mathbf{W}_k^\top \in \mathbb{R}^{d,d}$. This equation shows that the linear transformation $\mathbf{W}_q$ and $\mathbf{W}_k$ are always combined to compute attention scores with one single matrix $\mathbf{W}_{qk}$. While the matrices $\mathbf{W}_q$ and $\mathbf{W}_k$ are defined separately for computational efficiency, this formulation remains mathematically equivalent [see also Elhage et al., 2021, Olsson et al., 2022, Dar et al., 2023].

We observe that $\mathbf{X}\mathbf{W}_{qk}\mathbf{X}^\top$ corresponds to a bilinear form (see Definition S1.2). Specifically, the entry $\hat{\alpha}_{ij} = [\hat{\mathbf{A}}]_{ij}$ can be formulated in two equivalent ways: (1) as the canonical dot product between a query $\mathbf{q}_i$ and a key $\mathbf{k}_j$ (like in standard Transformer models), or (2) as the dot product between tokens $\mathbf{x}_i$ and $\mathbf{x}_j$ under the bilinear form $\mathbf{W}_{qk}$,

$$\hat{\alpha}_{ij} = \langle \mathbf{q}_i, \mathbf{k}_j \rangle = \langle \mathbf{x}_i, \mathbf{W}_{qk}\mathbf{x}_j \rangle = \langle \mathbf{x}_i, \mathbf{x}_j \rangle_{\mathbf{W}_{qk}}. \quad (2)$$

Intuitively, this indicates that $\mathbf{W}_q$ and $\mathbf{W}_k$ define an alternative metric $\mathbf{W}_{qk}$ in the embedding space, which quantifies the score of $\mathbf{x}_i$ and $\mathbf{x}_j$ without requiring explicit query and key vectors. We formalize this intuition in the following,

Proposition 2.1. *(Self-attention scores preserve the structure of geometrical projections). Let $\mathbf{X} \in \mathbb{R}^{N,d}$ be the embedding of a sequence of N tokens such that $\mathbf{X} = [\mathbf{x}_0^\top, \mathbf{x}_1^\top, \ldots, \mathbf{x}_N^\top]$ and $\mathbf{x}_i \in \mathbb{R}^d \ \forall i$. Let $\mathbf{A}$ be the matrix of attention scores, and let $\alpha_{ij} = [\mathbf{A}]_{ij}$ be the (i, j) element of the attention matrix. We define $\mathbf{W}_{qk} = \mathbf{W}_q \mathbf{W}_k^\top$. The self-attention transformation maps the i-th token $\mathbf{x}_i$ into $\hat{\mathbf{x}}_i$ as follows,*

$$\hat{\mathbf{x}}_i^\top = \mathbf{x}_i^\top + \sum_{j=1}^{N} \alpha_{ij} \mathbf{x}_j \mathbf{W}_v, \quad (3)$$

where the coefficients $\{\alpha_{ij}\}$ represent a convex combination of $\mathbf{x}_j$ within the subspace spanned by $\mathbf{X} =$

$\{\mathbf{x}_0^\top, \mathbf{x}_1^\top, \ldots, \mathbf{x}_N^\top\}$. *These coefficients preserve the ordering of the geometrical projection of* $\mathbf{x}_i$ *onto the subspace* $\mathbf{X}$ *given by the bilinear form* $\mathbf{W}_{qk}$,

$$\hat{\alpha}_{ij}(\mathbf{W}_{qk}) = \langle \mathbf{x}_i, \mathbf{W}_{qk}\mathbf{x}_j \rangle = \langle \mathbf{x}_i, \mathbf{x}_j \rangle_{\mathbf{W}_{qk}}, \quad (4)$$

such that,

$$\alpha_{ij} < \alpha_{ij'} \iff \hat{\alpha}_{ij} < \hat{\alpha}_{ij'} \quad \forall i, j, j'. \quad (5)$$

A proof of this proposition and its generalization for multi-head attention is in Appendix S1.2. The order of the attention scores is thereby preserved from the raw attention scores to the final attention scores (after soft-max).

It follows that $\mathbf{W}_{qk}$ defines the geometric structure that encodes the relevance of the token embedding $\mathbf{x}_j$ in predicting $\mathbf{x}_i$ through projections within the subspace (see Equation (3)). Therefore, token prediction depends on learning an optimal bilinear form $\mathbf{W}_{qk}$ to project tokens in the embedding space effectively. We note that $\mathbf{W}_v$ is a linear transformation that is applied independently to each projection in the sum and thus does not influence our derivation. In the following sections, we demonstrate how this equivalent formulation of self-attention provides a useful framework for analyzing the training of Transformer models. Specifically, we show that the choice of the objective function such as autoregressive prediction [Radford et al., 2019] or bidirectional training [Devlin et al., 2019] produces distinct structural patterns in $\mathbf{W}_{qk}$.

2.2. Deriving the gradients of self-attention with bilinear forms

To show the connection between the objective function and the structures of self-attention matrices, we derive a convenient formulation for the weight update of $\mathbf{W}_{qk}$. We first formulate a sequence modeling problem with self-supervised training as follows. Let $U = \{t_1, \ldots, t_N\}$ be a sequence of N tokens from a vocabulary of dimension V. Let $\mathcal{L}(U)$ be the negative log-likelihood of each token t_i, expressed as

$$\mathcal{L}(U; \mathcal{W}) = \sum_i \mathcal{L}(t_i) = -\sum_i \log p(t_i \,|\, \{t_j : j \in C_i\}; \mathcal{W}),$$
$$(6)$$

where $\mathcal{W}$ is the set of trainable parameters, and $C_i \subset [0, 1, \ldots, N]$ is the set of indices defining the set of tokens $\{t_j\}$ of the conditional probability distribution. This allows us to isolate the contribution of each token t_j to the prediction of the target token t_i. Here,
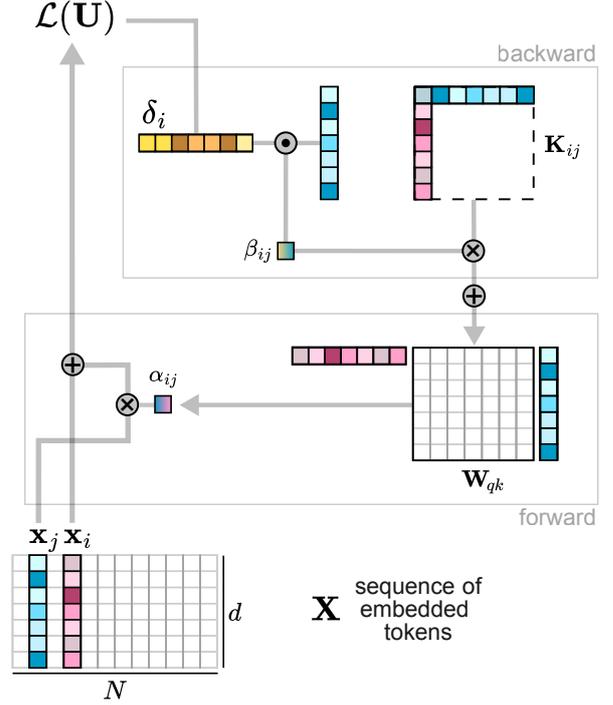

Figure 1: Illustration of the computation of the self-attention score between token $\mathbf{x}_i$ and token $\mathbf{x}_j$ (forward pass, see Equation (3)), and its corresponding contribution to the weight update of $\mathbf{W}_{qk}$ (backward pass, see Equation (8)). The symbols "$\oplus$", "$\otimes$", and "$\odot$" refer to the addition, multiplication, and dot product operations, respectively.

we demonstrate that the updates to the matrix $\mathbf{W}_{qk}$ follow a structured pattern: the contribution of the token t_j in the prediction of the embedding t_i results in adding a rank-1 matrix $\mathbf{K}_{ij}$ to the matrix $\mathbf{W}_{qk}$. As a result, the total weight update to $\mathbf{W}_{qk}$ is expressed as a linear combination of these rank-1 matrices. We formalize this observation in the following proposition.

Proposition 2.2. *(The implicit weight update as sum of rank-1 matrices). Let* $U = \{t_1, \ldots, t_N\}$ *be a sequence of N tokens, and let* $\mathcal{L}(U)$ *be the negative log-likelihood*

$$\mathcal{L}(U; \mathcal{W}) = \sum_i \mathcal{L}(t_i) = -\sum_i \log p(t_i \,|\, \{t_j : j \in C_i\}; \mathcal{W}),$$
$$(7)$$

with the conditional probability modeled with a Transformer model with learnable parameters $\mathcal{W}$. *Let the self-attention function be defined with a bilinear form as in Equation (1). Following the gradient of* $\mathcal{L}(U)$, *the implicit weight update of* $\mathbf{W}_{qk}^l$ *at the l-th layer is proportional to the sum of the contributions*

3

of each $t_j \in C_i$ in predicting t_i, as follows,

$$\Delta \mathbf{W}_{qk}^l \propto \sum_i \sum_{j \in C_i} \Delta \mathbf{W}_{qk}^l \Big|_{t_i \leftarrow t_j} = \sum_i \sum_{j \in C_i} \beta_{ij}^l \mathbf{K}_{ij}^{l-1} \quad (8)$$

or equivalently to the sum of the contribution of each $t_i \in P_j$ when predicted by t_j,

$$\Delta \mathbf{W}_{qk}^l \propto \sum_{i \in P_j} \sum_j \Delta \mathbf{W}_{qk}^l \Big|_{t_i \leftarrow t_j} = \sum_{i \in P_j} \sum_j \beta_{ij}^l \mathbf{K}_{ij}^{l-1} , \quad (9)$$

where β_{ij}^l is a scalar given by the contribution of the token embedding $\mathbf{x}_j$ to the error in predicting the token embedding $\mathbf{x}_i$ at the l-th self-attention layer, and where $\mathbf{K}_{ij}^{l-1} \in \mathbb{M}_d$ is a rank-1 matrix given by the outer product of the token embeddings at the previous layers $l - 1$,

$$\mathbf{K}_{ij}^{l-1} = \mathbf{x}_i^{l-1} \mathbf{x}_j^{l-1 \top} . \quad (10)$$

We provide proof for this proposition with related remarks in Appendix S1.3, and an illustrative description of the forward and backward pass in Figure 1.

2.3. The relation between objective functions and structures in self-attention matrices

Finally, we show how the formulation of $\Delta \mathbf{W}_{qk}$ enables the analysis of the contribution of any given token t^* to the weight updates, how this affects the properties of $\mathbf{W}_{qk}$, and how to relate these properties to the specific objective function. Indeed, Proposition 2.2 indicates that a token t^* impacts the updates of $\mathbf{W}_{qk}$ differently when serving as context for predicting other tokens or being itself predicted. When a token t^* serves as context ($t_j = t^*$), the embeddings of all predicted tokens contribute to the column space of $\mathbf{W}_{qk}$, where the update of the k-th column $\mathbf{w}_{\cdot,k}$ is given by

$$\Delta \mathbf{w}_{\cdot,k} \Big|_{t_j = t^*} = [\mathbf{x}_{t^*}]_k \left(\sum_{i \in P_t} \beta_{ij} \mathbf{x}_i \right) . \quad (11)$$

Only the embedding of t^* is instead added to the row space, where the update of the m-th row $\Delta \mathbf{w}_{m,\cdot}$ is given by

$$\Delta \mathbf{w}_{m,\cdot} \Big|_{t_i = t^*} = \left(\sum_{i \in P_t} \beta_{ij} [\mathbf{x}_i]_k \right) \mathbf{x}_{t^*} . \quad (12)$$

Intuitively, using t^* as context increases the dimensionality of the column space proportionally to the

embeddings of the predicted tokens, while reducing the row space along the direction of the embedding of t^*. Conversely, when t^* is being predicted ($t_i = t^*$), all token embeddings from the context are added to the row space of $\mathbf{W}_{qk}$, while only the embedding of t^* is added to the column space. Importantly, any token t^* is used differently as context or as prediction depending on the training objective. Autoregressive training implicitly introduces directionality by predicting each token based solely on its preceding tokens. In contrast, bidirectional training uses tokens as context and as predictions symmetrically. This fundamental difference between the two objective functions affects the weight updates of $\mathbf{W}_{qk}$, and in turn, the structures encoded in its columns and rows. We describe this in the following two informal Theorems.

Theorem 2.3. *(Informal) (**Autoregressive training leads to directional weight upates**). Let $\Delta \mathbf{W}_{qk}$ be the weight update from Proposition 2.2, derived from an autoregressive objective function. There are, on average, more columns with high norms than rows with high norms, that is, there exist a $\gamma \in \mathbb{R}$ such that,*

$$Pr[\|\mathbf{w}_{\cdot,k}\| > w] > Pr[\|\mathbf{w}_{m,\cdot}\| > w] \quad \forall w > \gamma , \quad (13)$$

for any k-th column and m-th row, thereby inducing column dominance.

Theorem 2.4. *(Informal) (**Bidirectional training leads to symmetric weight upates**). Let U be an ordered sequence of N tokens $U = [t_1, \ldots, t_N]$. Let $\Delta \mathbf{W}_{qk}$ be the weight update from Proposition 2.2, derived from a bidirectional objective function. Every pair (i, j) with $i \neq j$ contributes to the weight update with a term that is approximately symmetric,*

$$\Delta \mathbf{W}_{qk} \Big|_{t_i \leftrightarrow t_j} \approx \Delta \mathbf{W}_{qk}^\top \Big|_{t_i \leftrightarrow t_j} , \quad (14)$$

thereby inducing symmetric structures.

We provide a formal definition and proof of these two Theorems, and the related Propositions and Lemmas in Appendix S1.4.

3. Symmetric and directional structures are predominant in Transformer models

In this section, we validate our theoretical findings by quantifying empirically the degree of symmetry and directionality in different families of open-source
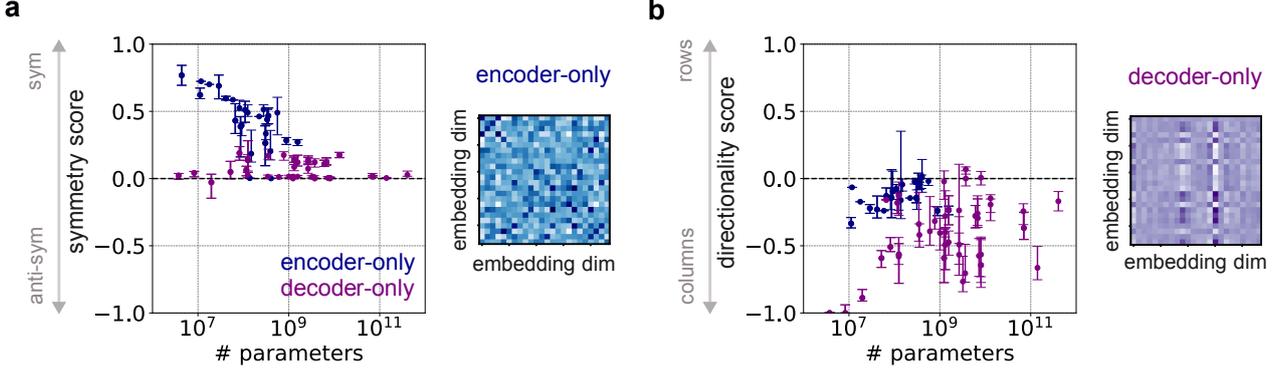
4

Figure 2: **a**) Left) Median symmetry score of the matrix $\mathbf{W}_{qk}$ as a function of the total number of parameters. Each dot corresponds to the median and the interquartile range across layers of a given pre-trained model (see Tables in Appendix S3). Right) Example of structures in the $\mathbf{W}_{qk}$ matrix of an encoder-only model (BERT Tiny, layer 1 [Turc et al., 2019]) **b**) Left) Same as in **a** for the median directionality score of the matrix $\mathbf{W}_{qk}$. Right) Example of structures in the $\mathbf{W}_{qk}$ matrix of a decoder-only model (TinyStories GPT, layer 1 [Eldan and Li, 2023])

Transformer models. To do so, we define two scores for symmetry and directionality in square matrices. First, we define the symmetry score $s \in \mathbb{R}$ as follows,

Definition 3.1. (*Symmetry score*). Given a square matrix $\mathbf{M} \in \mathbb{M}_n$ we define the symmetry score,

$$s = 2\frac{\|\mathbf{M}_s\|_F^2 - \|\mathbf{M}_n\|_F^2}{\|\mathbf{M}\|_F^2}, \quad (15)$$

where $\| \cdot \|_F$ is the Frobenious norm, and $\mathbf{M}_s$ and $\mathbf{M}_n$ are the symmetric and skew-symmetric parts of the Toeplitz decomposition of $\mathbf{M}$, respectively,

$$\mathbf{M}_s = \frac{1}{2}(\mathbf{M} + \mathbf{M}^\top) \quad ; \quad \mathbf{M}_n = \frac{1}{2}(\mathbf{M} - \mathbf{M}^\top). \quad (16)$$

Here, positive and negative symmetry scores indicate the presence of symmetric and skew-symmetric structures, respectively (see Appendix S1.5). Second, we define the directionality score $d \in \mathbb{R}$ as follows,

Definition 3.2. (*Directionality score*). Given a square matrix $\mathbf{M} \in \mathbb{M}_n$ we define the directionality score,

$$d = \frac{\bar{r}_{\mathbf{M}} - \bar{c}_{\mathbf{M}}}{\bar{r}_{\mathbf{M}} + \bar{c}_{\mathbf{M}}}, \quad (17)$$

where $\bar{c}_{\mathbf{M}}$ is the sum of the norm of the columns that are higher than a given threshold, as follows,

$$\bar{c}_{\mathbf{M}} = \sum_{k \in \overline{C}} \|\mathbf{m}_{\cdot,k}\|_2 \text{ with } \overline{C} = \{k \mid \|\mathbf{m}_{\cdot,k}\|_2 > \mu_c + \gamma\sigma_c\}, \quad (18)$$

where $\| \cdot \|_2$ is the L2 norm, $\|\mathbf{m}_{\cdot,k}\|_2$ is the norm of the k-th column, $\mu_c = \mathbb{E}[\|\mathbf{m}_{\cdot,k}\|_2]$ and $\sigma_c = \sqrt{\mathrm{Var}\|\mathbf{m}_{\cdot,k}\|_2}$ are the mean and standard deviation of the column norms, γ is a scaling factor, and similarly $\bar{r}_{\mathbf{M}}$ is the sum of the norm of the rows that are higher than a given threshold,

$$\bar{r}_{\mathbf{M}} = \sum_{k \in \overline{\mathcal{R}}} \|\mathbf{m}_{k,\cdot}\|_2 \text{ with } \overline{\mathcal{R}} = \{k \mid \|\mathbf{m}_{k,\cdot}\|_2 > \mu_r + \gamma\sigma_r\}, \quad (19)$$

with $\|\mathbf{m}_{k,\cdot}\|_2$ as the norm of the k-th row, $\mu_r = \mathbb{E}[\|\mathbf{m}_{k,\cdot}\|_2]$ and $\sigma_r = \sqrt{\mathrm{Var}\|\mathbf{m}_{k,\cdot}\|_2}$ as the mean and standard deviation of the row norms.

Here, positive and negative directionality scores indicate the dominance of high norm rows or columns, respectively (see Appendix S1.6). Finally, we compute the matrix $\mathbf{W}_{qk}$ for every layer, calculate the median symmetry and directionality score across layers, and analyze the differences between encoder- and decoder-only variants.

We find that encoder-only models remarkably show a higher degree of symmetry than decoder-only (Figure 2a). This difference is consistent across multiple families of models and input modalities, such as BERT [Devlin et al., 2019], GPT [Radford et al., 2018, 2019], LLAMA3 [Touvron et al., 2023], Phi [Hughes, 2023, Abdin et al., 2024], MISTRAL [Jiang et al., 2023], ModernBERT [Warner et al., 2024], and many others (see Figure S1 for vision and audio models). Strikingly, we observe that decoder-only models have higher degrees of directionality than encoder-only models (Figure 2b). Again, this difference is

5

consistent across all the models and input modalities we consider. We show in Figure S2 that a similar pattern is observed when including full encoder-decoder Transformers (e.g. the language T5 models [Xue et al., 2021]), despite these models having an overall lower degree of directionality.

4. Experiments

In this final section, we test if using structural priors based on our previous results can improve the pre-training of Transformer models. To do so, we train Transformer models from scratch and perform a series of experiments to analyze how symmetric and directional structures develop during training across layers.

4.1. Evolution of symmetric and directional structures during learning

To test the applicability of our result, we first train 12-layer transformer models in both encoder and decoder modes and quantify the median symmetry and directionality scores across epochs. At initialization, the symmetry and directionality score of the matrix $\mathbf{W}_{qk}$ at any layer is zero (see Definition 3.1 and Definition 3.2 and related Appendix S1.5 and S1.6). The incremental update of $\mathbf{W}_{qk}$ we described in the previous sections predicts that decoder-only models develop high-norm columns incrementally during training (see Theorem 2.3). Likewise, as symmetric weight updates are added to $\mathbf{W}_{qk}$ in encoder-only models, Theorem 2.4 predicts that symmetric structures emerge incrementally during training.

Consistent with our results on pre-trained models, encoder-only models show a higher degree of symmetry than decoder-only models (Figure 3a). In contrast, decoder-only models have a higher directionality score (Figure 3b). We observe this difference on all datasets we tested (Jigsaw [cjadams et al., 2017], Wikipedia [Foundation, 2022], Red Pajama [Computer, 2023], see Figure S3). Furthermore, late layers of encoder-only models are more symmetric and converge faster than early layers when training bidirectionally. At the same time, decoder-only models learn almost non-symmetric matrices with strong skew-symmetric matrices in the middle layers (Figure 3c). When training unidirectionally, both encoder and decoder models show a higher degree of directionality for late layers, which is remarkably stronger for decoder-only models (Figure 3d). We observe

Table 1: The final loss at the end of training and the speed-up for the 4 and 12-layer models trained on the Jigsaw dataset [cjadams et al., 2017], Wikipedia [Foundation, 2022], and Red Pajama [Computer, 2023], with and without symmetry initialization (see Appendix S2.1). Speed-up (%) is calculated by subtracting the epoch at which the symmetrically initialized model reaches the non-symmetric model's final loss from the total number of epochs, and then dividing by the total number of epochs. For example, a 50% speed-up means that the model with symmetric initialization achieves the final loss of the non-symmetric model in half the number of training epochs.

MODEL	LOSS	SPEED-UP
4-LAYER MODEL		
JIGSAW	2.782	
JIGSAW (+ SYMM)	**2.758**	26 %
WIKIPEDIA	0.984	
WIKIPEDIA (+ SYMM)	**0.812**	73 %
RED PAJAMA	1.106	
RED PAJAMA (+ SYMM)	**0.907**	69 %
12-LAYER MODEL		
JIGSAW	1.419	
JIGSAW (+ SYMM)	1.430	0 %
WIKIPEDIA	0.256	
WIKIPEDIA (+ SYMM)	**0.247**	20 %
RED PAJAMA	0.297	
RED PAJAMA (+ SYMM)	**0.274**	35 %

similar differences across layers with all the datasets we tested (Figure S4), despite these models having less significant differences in directionality scores. See Appendix S2 for a detailed description of the experiments.

4.2. Enforcing symmetry at initialization improves the training of encoder-only models

The previous section showed that symmetric structures incrementally emerge during training in the $\mathbf{W}_{qk}$ matrices of encoder-only models. Here, we first provide evidence that these findings can be exploited to speed up training using symmetry as an inductive bias. Specifically, we explore how symmetric initialization influences the training dynamics of the model
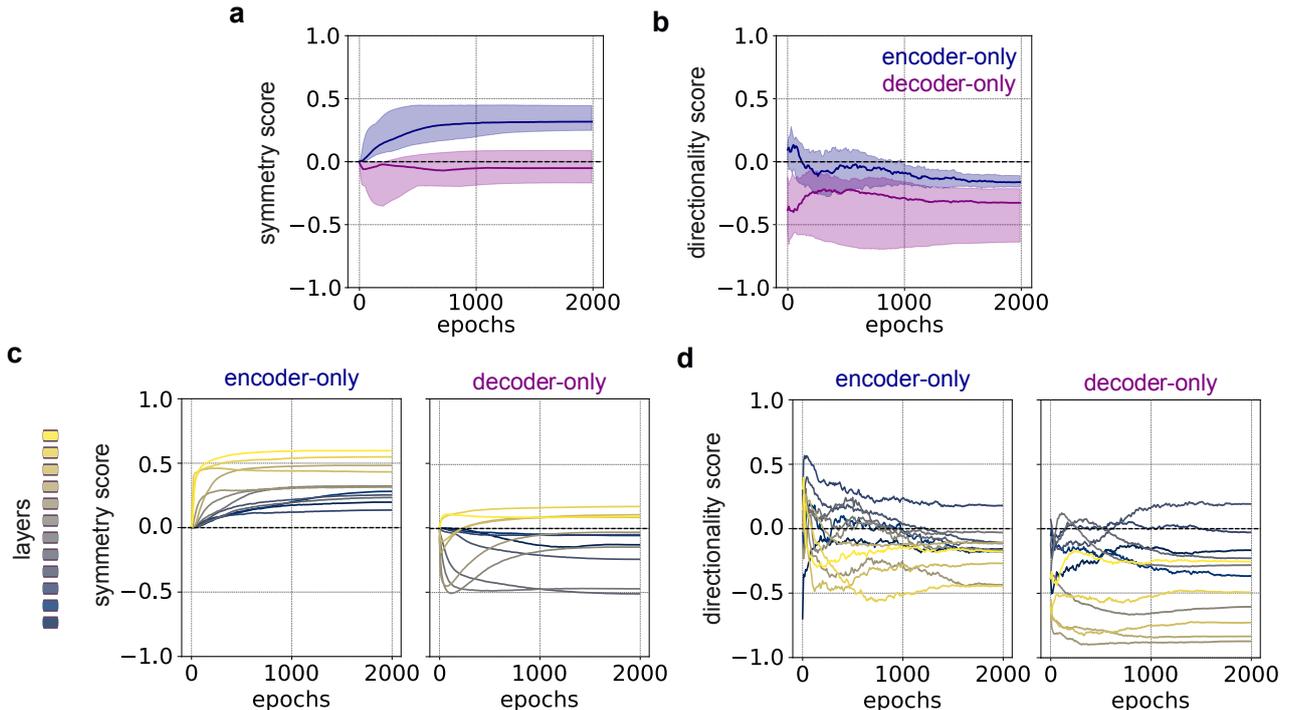
Figure 3: **a**) Evolution of symmetry score during training. Shown are the median and the interquartile range. Models were trained on the Wikipedia dataset [Foundation, 2022]. Encoder-only and decoder-only models are color-coded in blue and purple, respectively (see legend). **b**) Same as in panel **a** for the median directionality score. **c**) Evolution of the median symmetry score across layers of the encoder-only (left) and decoder-only (right) models. Each layer is color-coded as shown on the legend. **d**) Same as panel **c** for the median directionality score.

and whether it enhances learning efficiency and overall performance.

We train 4-layer and 12-layer encoder-only models, comparing two initialization strategies: initialize the self-attention matrices independently versus initializing the $\mathbf{W}_q$ and $\mathbf{W}_k$ in each self-attention layer to ensure that $\mathbf{W}_{qk}$ is symmetric (see Appendix S2). We report the results of our experiments in Table 1. We observe that enforcing symmetry at initialization leads to lower loss values at the end of training for most of the models. Importantly, symmetric initialization significantly accelerates convergence, reaching the final loss value faster than those with random initialization (up to 75% faster for 4-layer models and 35% faster for 12-layer models, see also Figure S5a). Moreover, we observe that self-attention matrices initialized symmetrically lose symmetry during training but converge to higher symmetry levels than random initialization (Figure S5b) This symmetric initialization decreases the gap in symmetric scores between layers compared to random initialization (Figure S5c). These results highlight that

embedding symmetry as an inductive bias across all Transformer layers can enhance training efficiency and model performance.

5. Related work

Mechanistic Interpretability (MI) In contrast to interpretability approaches that focus on explaining specific data instances by analyzing features [Wu et al., 2020, Lundstrom et al., 2022], attention scores [Hoover et al., 2020, Barkan et al., 2021, Yeh et al., 2023], or output variations [Jin et al., 2020, Wang et al., 2022a], mechanistic interpretability (MI) seeks to provide a more general understanding of Transformer models. MI is based on the study of "circuits," analyzing the between activations across different components of a Transformer [Olah et al., 2020]. Following the categorization by [Rai et al., 2024], MI techniques include: (i) The *logit lens* [nostalgebraist, 2020, Geva et al., 2021] projects layer activations or weights into the vocabulary space $\mathcal{V}$, allowing the derivation of logits and revealing the influence of in-

dividual components on the prediction. This technique can also be applied to query-key matrices $\mathbf{W}_{qk}$ to study how attention heads transform source into target tokens [Dar et al., 2023]; (ii) *Probing techniques* allow to identify correlations between layer activations and features by training a linear classifier or shallow neural network (the probe) to predict the presence of a feature in layer activations [Dalvi et al., 2019, Gurnee et al., 2023]; (iii) *Sparse autoencoders* map activations into a higher-dimensional yet sparse representation, facilitating the identification of independent (monosemantic) features [Huben et al., 2024, Bricken et al., 2023]; (iv) *Visualization techniques* facilitate the analysis of attention scores [Olsson et al., 2022, Lieberum et al., 2023] and neuronal activity patterns [Elhage et al., 2022] by rendering them in a graphical format. However, their utility often depends on human comprehension of the resulting visualizations; (v) *Ablation studies* assess the importance of model components by systematically removing or modifying them and observing the resulting behavioral changes [Olsson et al., 2022, Wang et al., 2022b]; (vi) *Causal mediation analysis (CMA)* analyzes the importance of components [Vig et al., 2020, Meng et al., 2022] or connections [Wang et al., 2022b, Goldowsky-Dill et al., 2023] between them by introducing perturbations (e.g., noise) and selectively patching them to measure the recovery of lost capabilities. Our work adds a new perspective on MI by providing a scalable and generalizable approach to the mechanistic understanding of self-attention. In contrast to existing work, it is not limited to analyzing fully trained models but investigates the influence of learning and can analyze models of different sizes across all modalities.

MI for model enhancement Insights from MI have been instrumental in various applications, including improving model safety [Belrose et al., 2023], updating the model's learned knowledge [Meng et al., 2022], and guiding the generation process of generative models [Geva et al., 2022]. One of the most exciting applications is leveraging MI techniques to improve model performance. For instance, [Marks et al., 2024] identify and eliminate spurious features, leading to improved generalization in classification tasks. Similarly, [Trockman and Kolter, 2023] observe that query-key matrices ($\mathbf{W}_{qk}$) frequently exhibit a pronounced negative diagonal, prompting them to initialize it with approximately the identity matrix, leading to enhanced accuracy in

image classification tasks. Similar to [Trockman and Kolter, 2023], we demonstrate that findings about the structure of $\mathbf{W}_{qk}$ can inform initialization strategies that improve Transformer performance. However, since the identity matrix is one instance of a symmetric matrix, we consider the work by [Trockman and Kolter, 2023] as a special instance of our broader approach, confirming our findings in the image domain.

6. Discussion

In this work, we demonstrate how bidirectional and autoregressive objective functions influence the structure of the query-key matrix $\mathbf{W}_{qk}$ in self-attention, enhancing our understanding of Transformer models. Our mathematical framework shows that bidirectional training induces symmetric structures in $\mathbf{W}_{qk}$, whereas autoregressive training results in matrices characterized by directionality and column dominance. To empirically validate our analysis, we develop and apply symmetry and directionality scores to various Transformer encoder and decoder models across multiple modalities, including text, audio, and images. Our results reveal that bidirectionally trained encoder models exhibit high symmetry, while autoregressively trained decoder models demonstrate strong directionality, thereby supporting the predictions of our mathematical framework. This suggests that self-attention inherently reflects these structural properties, contributing to the mechanistic interpretability of Transformer models. Finally, we leverage our findings to improve convergence speed during bidirectional training by initializing $\mathbf{W}_q$ and $\mathbf{W}_k$ matrices such that $\mathbf{W}_{qk}$ is symmetric.

While our findings mark an initial step toward leveraging symmetry for more efficient Transformer training, further research is required to assess the scalability of symmetric initialization in large-scale models and across diverse domains. Furthermore, it is important to explore strategies for leveraging the directionality structures of decoder-only models. For instance, incorporating structural constraints into the objective function or weight regularization could enhance training efficiency and stability in autoregressive settings. By bridging theoretical insights with practical improvements, our work not only advances the interpretability of self-attention but also provides a foundation for optimizing Transformer architectures. Ultimately, these findings contribute to a deeper understanding of the mechanisms governing

self-attention, paving the way for more reliable and efficient Transformer-based models.

Authorship contributions

Conceptualization: MS, TS, BG. Mathematical analysis: MS, PVA. Analysis of pre-trained models: MS, PS. Experiments: PS. Writing: MS, PS, BG. Supervision: TS, BG.

Code availability

The code to reproduce our results and all the Figures in the main text and Supplementary Materials is freely available at github.com/matteosaponati/attention-geometry.

Declaration of Interests

The authors declare no competing interests.

References

Marah Abdin, Jyoti Aneja, Hany Awadalla, Ahmed Awadallah, Ammar Ahmad Awan, Nguyen Bach, Amit Bahree, Arash Bakhtiari, Jianmin Bao, Harkirat Behl, et al. Phi-3 Technical Report: A Highly Capable Language Model Locally on Your Phone, August 2024. arXiv:2404.14219.

Hangbo Bao, Li Dong, Songhao Piao, and Furu Wei. BEiT: BERT Pre-Training of Image Transformers. In *Proceedings of the 10th International Conference on Learning Representations*, ICLR, 2022. URL https://openreview.net/forum?id=p-BhZSz59o4.

Oren Barkan, Edan Hauon, Avi Caciularu, Ori Katz, Itzik Malkiel, Omri Armstrong, and Noam Koenigstein. Grad-SAM: Explaining Transformers via Gradient Self-Attention Maps. In *Proceedings of the 30th ACM International Conference on Information & Knowledge Management*, CIKM, page 2882–2887, Virtual Event Queensland Australia, October 2021. ACM. ISBN 978-1-4503-8446-9. doi: 10.1145/3459637.3482126.

Nora Belrose, Zach Furman, Logan Smith, Danny Halawi, Igor Ostrovsky, Lev McKinney, Stella Biderman, and Jacob Steinhardt. Eliciting Latent Predictions from Transformers with the Tuned Lens, March 2023. arXiv:2303.08112.

Sid Black, Gao Leo, Phil Wang, Connor Leahy, and Stella Biderman. GPT-Neo: Large Scale Autoregressive Language Modeling with Mesh-Tensorflow. In *GPT-Neo: Large Scale Autoregressive Language Modeling with Mesh-Tensorflow*. Zenodo, March 2021. doi: 10.5281/ZENODO.5297715.

Trenton Bricken, Adly Templeton, Joshua Batson, Brian Chen, Adam Jermyn, Tom Conerly, Nick Turner, Cem Anil, Carson Denison, Amanda Askell, et al. Towards Monosemanticity: Decomposing Language Models With Dictionary Learning. *Transformer Circuits Thread*, October 2023. URL https://transformer-circuits.pub/2023/monosemantic-features/index.html.

cjadams, Jeffrey Sorensen, Julia Elliott, Lucas Dixon, Mark McDonald, nithum, and Will Cukierski. Toxic Comment Classification Challenge, 2017. URL https://kikiaggle.com/competitions/jigsaw-toxic-comment-classification-challenge.

Together Computer. RedPajama: an Open Dataset for Training Large Language Models. https://github.com/togethercomputer/RedPajama-Data, October 2023.

Fahim Dalvi, Nadir Durrani, Hassan Sajjad, Yonatan Belinkov, Anthony Bau, and James Glass. What Is One Grain of Sand in the Desert? Analyzing Individual Neurons in Deep NLP Models. *Proceedings of the AAAI Conference on Artificial Intelligence*, 33(01):6309–6317, July 2019. ISSN 2374-3468. doi: 10.1609/aaai.v33i01.33016309.

Guy Dar, Mor Geva, Ankit Gupta, and Jonathan Berant. Analyzing Transformers in Embedding Space. In *Proceedings of the 61st Annual Meeting*

of the Association for Computational Linguistics, volume 1 of *ACL*, page 16124–16170, Toronto, Canada, 2023. Association for Computational Linguistics. doi: 10.18653/v1/2023.acl-long.893.

Jacob Devlin, Ming-Wei Chang, Kenton Lee, and Kristina Toutanova. BERT: Pre-training of Deep Bidirectional Transformers for Language Understanding. In *Proceedings of the 2019 Conference of the North American Chapter of the Association for Computational Linguistics*, volume 1 of *NAACL*, page 4171–4186, Minneapolis, Minnesota, 2019. Association for Computational Linguistics. doi: 10.18653/v1/N19-1423.

Alexey Dosovitskiy, Lucas Beyer, Alexander Kolesnikov, Dirk Weissenborn, Xiaohua Zhai, Thomas Unterthiner, Mostafa Dehghani, Matthias Minderer, Georg Heigold, Sylvain Gelly, et al. An Image is Worth 16x16 Words: Transformers for Image Recognition at Scale. In *Proceedings of the 9th International Conference on Learning Representations*, ICLR, 2021. URL https://openreview.net/forum?id=YicbFdNTTy.

Ronen Eldan and Yuanzhi Li. TinyStories: How Small Can Language Models Be and Still Speak Coherent English?, May 2023. arXiv:2305.07759.

Nelson Elhage, Neel Nanda, Catherine Olsson, Tom Henighan, Nicholas Joseph, Ben Mann, Amanda Askell, Yuntao Bai, Anna Chen, Tom Conerly, et al. A Mathematical Framework for Transformer Circuits. *Transformer Circuits Thread*, December 2021. URL https://transformer-circuits.pub/2021/framework/index.html.

Nelson Elhage, Tristan Hume, Catherine Olsson, Neel Nanda, Tom Henighan, Scott Johnston, Sheer ElShowk, Nicholas Joseph, Nova DasSarma, Ben Mann, et al. Softmax Linear Units. *Transformer Circuits Thread*, June 2022. URL https://transformer-circuits.pub/2022/solu/index.html.

Wikimedia Foundation. Wikimedia Downloads. https://dumps.wikimedia.org, 2022.

Mor Geva, Roei Schuster, Jonathan Berant, and Omer Levy. Transformer Feed-Forward Layers Are Key-Value Memories. In *Proceedings of the 2021 Conference on Empirical Methods in Natural Language Processing*, EMNLP, page 5484–5495, Online and Punta Cana, Dominican Republic, November 2021. Association for Computational Linguistics. doi: 10.18653/v1/2021.emnlp-main.446.

Mor Geva, Avi Caciularu, Kevin Wang, and Yoav Goldberg. Transformer Feed-Forward Layers Build Predictions by Promoting Concepts in the Vocabulary Space. In *Proceedings of the 2022 Conference on Empirical Methods in Natural Language Processing*, EMNLP, page 30–45, Abu Dhabi, United Arab Emirates, December 2022. Association for Computational Linguistics. doi: 10.18653/v1/2022.emnlp-main.3.

Nicholas Goldowsky-Dill, Chris MacLeod, Lucas Sato, and Aryaman Arora. Localizing Model Behavior with Path Patching, April 2023. arXiv:2304.05969.

Wes Gurnee, Neel Nanda, Matthew Pauly, Katherine Harvey, Dmitrii Troitskii, and Dimitris Bertsimas. Finding Neurons in a Haystack: Case Studies with Sparse Probing. *Transactions on Machine Learning Research (TMLR)*, 2023. ISSN 2835-8856. URL https://openreview.net/forum?id=JYs1R9IMJr.

Benjamin Hoover, Hendrik Strobelt, and Sebastian Gehrmann. exBERT: A Visual Analysis Tool to Explore Learned Representations in Transformer Models. In *Proceedings of the 58th Annual Meeting of the Association for Computational Linguistics: System Demonstrations*, ACL, page 187–196, Online, 2020. Association for Computational Linguistics. doi: 10.18653/v1/2020.acl-demos.22.

Robert Huben, Hoagy Cunningham, Logan Riggs Smith, Aidan Ewart, and Lee Sharkey. Sparse Autoencoders Find Highly Interpretable Features in Language Models. In *Proceedings of the 12th International Conference on Learning Representations*, ICLR, 2024. URL https://openreview.net/forum?id=F76bwRSLeK.

Alyssa Hughes. Phi-2: The Surprising Power of Small Language Models, December 2023.

Albert Q. Jiang, Alexandre Sablayrolles, Arthur Mensch, Chris Bamford, Devendra Singh Chaplot, Diego de las Casas, Florian Bressand, Gianna Lengyel, Guillaume Lample, Lucile Saulnier, et al. Mistral 7B, October 2023. arXiv:2310.06825.

Di Jin, Zhijing Jin, Joey Tianyi Zhou, and Peter Szolovits. Is BERT Really Robust? A Strong

Baseline for Natural Language Attack on Text Classification and Entailment. *Proceedings of the AAAI Conference on Artificial Intelligence*, 34 (05):8018–8025, April 2020. ISSN 2374-3468. doi: 10.1609/aaai.v34i05.6311.

Zhenzhong Lan, Mingda Chen, Sebastian Goodman, Kevin Gimpel, Piyush Sharma, and Radu Soricut. ALBERT: A Lite BERT for Self-supervised Learning of Language Representations. In *Proceedings of the 8th International Conference on Learning Representations*, ICLR, 2020. URL https://openreview.net/forum?id=H1eA7AEtvS.

Tom Lieberum, Matthew Rahtz, János Kramár, Neel Nanda, Geoffrey Irving, Rohin Shah, and Vladimir Mikulik. Does Circuit Analysis Interpretability Scale? Evidence from Multiple Choice Capabilities in Chinchilla, July 2023. arXiv:2307.09458.

Yinhan Liu, Myle Ott, Naman Goyal, Jingfei Du, Mandar Joshi, Danqi Chen, Omer Levy, Mike Lewis, Luke Zettlemoyer, and Veselin Stoyanov. RoBERTa: A Robustly Optimized BERT Pretraining Approach, July 2019. arXiv:1907.11692.

Ilya Loshchilov and Frank Hutter. Decoupled Weight Decay Regularization. In *Proceedings of the 7th International Conference on Learning Representations*, ICLR, 2019. URL https://openreview.net/forum?id=Bkg6RiCqY7.

Daniel D. Lundstrom, Tianjian Huang, and Meisam Razaviyayn. A Rigorous Study of Integrated Gradients Method and Extensions to Internal Neuron Attributions. In *Proceedings of the 39th International Conference on Machine Learning*, volume 162 of *ICML*, page 14485–14508. PMLR, July 2022.

Samuel Marks, Can Rager, Eric J. Michaud, Yonatan Belinkov, David Bau, and Aaron Mueller. Sparse Feature Circuits: Discovering and Editing Interpretable Causal Graphs in Language Models, March 2024. arXiv:2403.19647.

Kevin Meng, David Bau, Alex Andonian, and Yonatan Belinkov. Locating and Editing Factual Associations in GPT. In *Advances in Neural Information Processing Systems (NeurIPS)*, volume 35, page 17359–17372. Curran Associates, Inc., 2022.

nostalgebraist. Interpreting GPT: the logit lens, 2020. URL https://www.lesswrong.com/posts/AcKRB8wDpdaN6v6ru/interpreting-gpt-the-logit-lens.

Chris Olah. Mechanistic Interpretability, Variables, and the Importance of Interpretable Bases, June 2022. URL https://transformer-circuits.pub/2022/mech-interp-essay/index.html.

Chris Olah, Nick Cammarata, Ludwig Schubert, Gabriel Goh, Michael Petrov, and Shan Carter. Zoom In: An Introduction to Circuits. *Distill*, 5(3): e00024.001, March 2020. ISSN 2476-0757. doi: 10.23915/distill.00024.001.

Catherine Olsson, Nelson Elhage, Neel Nanda, Nicholas Joseph, Nova DasSarma, Tom Henighan, Ben Mann, Amanda Askell, Yuntao Bai, Anna Chen, et al. In-context Learning and Induction Heads. *Transformer Circuits Thread*, 2022. URL https://transformer-circuits.pub/2022/in-context-learning-and-induction-heads/index.html.

Alec Radford, Karthik Narasimhan, Tim Salimans, and Ilya Sutskever. Improving Language Understanding by Generative Pre-Training, June 2018.

Alec Radford, Jeff Wu, Rewon Child, D. Luan, Dario Amodei, and I. Sutskever. Language Models Are Unsupervised Multitask Learners, 2019.

Alec Radford, Jong Wook Kim, Tao Xu, Greg Brockman, Christine Mcleavey, and Ilya Sutskever. Robust Speech Recognition via Large-Scale Weak Supervision. In *Proceedings of the 40th International Conference on Machine Learning*, volume 202 of *ICML*, pages 28492–28518. PMLR, July 2023.

Daking Rai, Yilun Zhou, Shi Feng, Abulhair Saparov, and Ziyu Yao. A Practical Review of Mechanistic Interpretability for Transformer-Based Language Models, July 2024. arXiv:2407.02646.

Hugo Touvron, Thibaut Lavril, Gautier Izacard, Xavier Martinet, Marie-Anne Lachaux, Timothée Lacroix, Baptiste Rozière, Naman Goyal, Eric Hambro, Faisal Azhar, et al. LLaMA: Open and Efficient Foundation Language Models, February 2023. arXiv:2302.13971.

Asher Trockman and J. Zico Kolter. Mimetic Initialization of Self-Attention Layers. In *Proceedings of the 40th International Conference on Machine*

Learning, volume 202 of *ICML*, pages 34456–34468. PMLR, 2023.

Iulia Turc, Ming-Wei Chang, Kenton Lee, and Kristina Toutanova. Well-Read Students Learn Better: On the Importance of Pre-training Compact Models, September 2019. arXiv:1908.08962.

Ashish Vaswani, Noam Shazeer, Niki Parmar, Jakob Uszkoreit, Llion Jones, Aidan N Gomez, Lukasz Kaiser, and Illia Polosukhin. Attention is All you Need. In *Advances in Neural Information Processing Systems*, volume 30 of *NeurIPS*. Curran Associates, Inc., 2017.

Jesse Vig, Sebastian Gehrmann, Yonatan Belinkov, Sharon Qian, Daniel Nevo, Yaron Singer, and Stuart Shieber. Investigating Gender Bias in Language Models Using Causal Mediation Analysis. In *Advances in Neural Information Processing Systems*, volume 33 of *NeurIPS*, page 12388–12401. Curran Associates, Inc., 2020.

Boxin Wang, Chejian Xu, Xiangyu Liu, Yu Cheng, and Bo Li. SemAttack: Natural Textual Attacks via Different Semantic Spaces. In *Findings of the Association for Computational Linguistics*, NAACL, page 176–205, Seattle, United States, 2022a. Association for Computational Linguistics. doi: 10.18653/v1/2022.findings-naacl.14.

Kevin Wang, Alexandre Variengien, Arthur Conmy, Buck Shlegeris, and Jacob Steinhardt. Interpretability in the Wild: A Circuit for Indirect Object Identification in GPT-2 Small, November 2022b. arXiv:2211.00593.

Yufei Wang, Wanjun Zhong, Liangyou Li, Fei Mi, Xingshan Zeng, Wenyong Huang, Lifeng Shang, Xin Jiang, and Qun Liu. Aligning Large Language Models with Human: A Survey, July 2023. arXiv:2307.12966.

Benjamin Warner, Antoine Chaffin, Benjamin Clavié, Orion Weller, Oskar Hallström, Said Taghadouini, Alexis Gallagher, Raja Biswas, Faisal Ladhak, Tom Aarsen, et al. Smarter, Better, Faster, Longer: A Modern Bidirectional Encoder for Fast, Memory Efficient, and Long Context Finetuning and Inference, December 2024.

Thomas Wolf, Lysandre Debut, Victor Sanh, Julien Chaumond, Clement Delangue, Anthony Moi, Pierric Cistac, Tim Rault, Rémi Louf, Morgan Funtowicz, et al. HuggingFace's Transformers: State-of-the-art Natural Language Processing, July 2020. arXiv:1910.03771.

Zhiyong Wu, Yun Chen, Ben Kao, and Qun Liu. Perturbed Masking: Parameter-free Probing for Analyzing and Interpreting BERT. In *Proceedings of the 58th Annual Meeting of the Association for Computational Linguistics*, ACL, page 4166–4176, Online, 2020. Association for Computational Linguistics. doi: 10.18653/v1/2020.acl-main.383.

Linting Xue, Noah Constant, Adam Roberts, Mihir Kale, Rami Al-Rfou, Aditya Siddhant, Aditya Barua, and Colin Raffel. mT5: A Massively Multilingual Pre-Trained Text-to-Text Transformer, March 2021. arXiv:2010.11934.

Yifan Yao, Jinhao Duan, Kaidi Xu, Yuanfang Cai, Zhibo Sun, and Yue Zhang. A survey on large language model (LLM) security and privacy: The Good, The Bad, and The Ugly. *High-Confidence Computing*, 4(2):100211, June 2024. ISSN 26672952. doi: 10.1016/j.hcc.2024.100211.

Catherine Yeh, Yida Chen, Aoyu Wu, Cynthia Chen, Fernanda Viégas, and Martin Wattenberg. AttentionViz: A Global View of Transformer Attention. *IEEE Transactions on Visualization and Computer Graphics*, page 1–11, 2023. ISSN 1077-2626. doi: 10.1109/TVCG.2023.3327163.

S1. Mathematical proofs

S1.1. Preliminaries

Following the notation in [Vaswani et al., 2017, Radford et al., 2018], we define a Transformer architecture as,

Definition S1.1. (***Transformer architecture***). Let $\mathbf{U} \in \mathbb{R}^{N,V}$ be a matrix representing the sequence of N one-hot encoded tokens of dimension V. A Transformer architecture consists of L stacked attention blocks, each one composed of a self-attention layer and a feedforward layer, as follows,

$$\begin{cases} \mathbf{X}_0(\mathbf{U}) = \mathbf{U}\mathbf{W_e} + \mathbf{W}_p \\ \begin{cases} \hat{\mathbf{X}}_l = \mathbf{X}_{l-1} + a_l(\mathbf{X}_{l-1}; \mathbf{W}_q^l, \mathbf{W}_k^l, \mathbf{W}_v^l) \\ \mathbf{X}_l = \hat{\mathbf{X}}_l + m_l(\hat{\mathbf{X}}_l; \mathbf{W}_1^l, \mathbf{W}_2^l) \end{cases} \quad \forall l \in [1, L] \\ \sigma(\mathbf{Z}) = \sigma(\mathbf{X}_L \mathbf{W_u}), \end{cases} \tag{S1}$$

where $\mathbf{W_e} \in \mathbb{R}^{V,d}$ represents the linear transformation from the vocabulary space to the embedding space of dimension d, $\mathbf{W_p} \in \mathbb{R}^{V,d}$ represents the positional encoding, $\mathbf{X}_0 \in \mathbb{R}^{N,d}$ is the initial embedding of the sequence, $a_l(\cdot)$ is a self-attention function given by

$$a(\mathbf{X}_{l-1}) = \mathbf{A}^l(\mathbf{X}_{l-1})\mathbf{V}^l(\mathbf{X}_{l-1}) \tag{S2}$$

where the matrix of attention scores $\mathbf{A}^l(\mathbf{X}_{l-1})$ is given by

$$\begin{cases} \mathbf{Q}^l(\mathbf{X}_{l-1}) = \mathbf{X}_{l-1}\mathbf{W}_q^l \\ \mathbf{K}^l(\mathbf{X}_{l-1}) = \mathbf{X}_{l-1}\mathbf{W}_k^l \\ \mathbf{A}^l(\mathbf{X}_{l-1}) = \sigma\left(\frac{1}{\sqrt{d}}\mathbf{Q}^l\mathbf{K}^{lT}\right), \end{cases} \tag{S3}$$

where $1/\sqrt{d}$ is a constant normalization factor, and $\mathbf{W}_q^l \in \mathbb{R}^{d,d}$ and $\mathbf{W}_k^l \in \mathbb{R}^{d,d}$ represent linear transformations within the embedding space, $\mathbf{V}^l(\mathbf{X}_{l-1}) = \mathbf{X}_{l-1}\mathbf{W}_v^l$ represents a linear transformation within the embedding space, $m_l(\cdot)$ is a position-wise feedforward layer with hidden dimension d_f and learnable matrices $\mathbf{W}_1^l \in \mathbf{R}^{d,d_f}$ and $\mathbf{W}_2^l \in \mathbf{R}^{d_f,d}$, $\mathbf{W_u} \in \mathbb{R}^{d,V}$ represents the linear transformation from the embedding space back to the vocabulary space, $\sigma(\cdot)$ is the row-wise softmax function, and $\sigma(\mathbf{Z}) \in \mathbb{R}^{N,V}$ is the estimated probability distribution over the vocabulary. We omit layer normalization and biases for simplicity (see also [Elhage et al., 2021]).

Furthermore, we use the following definition of a bilinear form,

Definition S1.2. (***Bilinear form***). A bilinear form on a vector space V over a field F is a map $M : V \times V \to F$ that is linear in each argument separately, that is,

$$\begin{aligned} M(a\mathbf{x} + b\mathbf{y}, \mathbf{z}) &= aM(\mathbf{x}, \mathbf{z}) + bM(\mathbf{y}, \mathbf{z}) \\ M(\mathbf{x}, a\mathbf{y} + b\mathbf{z}) &= aM(\mathbf{x}, \mathbf{y}) + bM(\mathbf{x}, \mathbf{z}), \end{aligned} \tag{S4}$$

for all $\mathbf{x}, \mathbf{y}, \mathbf{z} \in V$ and $a, b \in F$. Let $\{\mathbf{e}_1, \dots, \mathbf{e}_d\}$ be a basis for the vector space V. The matrix $\mathbf{M}$ such that $[\mathbf{M}]_{ij} = M(\mathbf{e}_i, \mathbf{e}_j)$ is the matrix of the bilinear form on this basis, and it follows

$$M(\mathbf{x}, \mathbf{y}) = \mathbf{x}^\top \mathbf{M}\mathbf{y} \tag{S5}$$

Finally, we provide the following definition of autoregressive and bidirectional training objectives,

Definition S1.3. (**Autoregressive and bidirectional objectives**) Let $U = \{t_1, \dots, t_N\}$ a sequence of tokens. The joint probability of U is factorized autoregressively as follows,

$$\Pr[U] = \Pr[t_1, \dots, t_N] = \Pi_{i=1}^{N} \Pr[t_i|t_1, \dots, t_{i-1}]. \tag{S6}$$

13

During autoregressive training, a model with set of parameters $\mathcal{W}$ is optimized to minimize the following negative log-likelihood

$$\mathcal{L}(U; \mathcal{W}) = -\sum_{i=1}^{N} \log p(t_i \,|\, \{t_j\} : j < i \,; \mathcal{W}) \,, \tag{S7}$$

where the conditional probabilities are modeled with learnable parameters $\mathcal{W}$. The join probability of U can also be factorized bidirectionally as follows,

$$\Pr[U] = \Pr[t_1, \ldots, t_N] = \Pi_{i=1}^{N} \Pr[t_i | t_1, \ldots, t_{i-1}, t_{i+1}, \ldots, t_N] \,. \tag{S8}$$

During bidirectional training, a model with set of parameters $\mathcal{W}$ is optimized to minimize the following negative log-likelihood

$$\mathcal{L}(U; \mathcal{W}) = -\sum_{i=1}^{N} \log p(t_i \,|\, \{t_j\} : j \neq i \,; \mathcal{W}) \,. \tag{S9}$$

In practice, only a subset $M \in [1, \ldots, N]$ of the tokens are predicted as in Masked Language Modelling (MLM) [see Devlin et al., 2019, Warner et al., 2024], leading to the following negative log-likelihood

$$\mathcal{L}(U; \mathcal{W}) = -\sum_{i \in M} \log p(t_i \,|\, \{t_j\} : j \notin M \,; \mathcal{W}) \,. \tag{S10}$$

S1.2. Proof of Proposition 2.1 and related remarks

Proof. Let $\mathbf{A}$ be the matrix of attention scores in a self-attention layer as in Definition S1.1. It follows that,

$$\hat{\mathbf{X}}(\mathbf{X}) = \mathbf{X} + \mathbf{A}(\mathbf{X})\mathbf{V}(\mathbf{X}) = \mathbf{X} + \sigma\left(\frac{1}{\sqrt{d}}\mathbf{X}\mathbf{W}_{qk}\mathbf{X}^T\right)\mathbf{X}\mathbf{W}_v \,, \tag{S11}$$

where $\mathbf{W}_{qk} = \mathbf{W}_q \mathbf{W}_k^\top$, and where we refer to a general layer in a Transformer model, omitting the subscript l. It follows that the entry $\alpha_{ij} = [\mathbf{A}]_{ij}$ of the attention score matrix is given by,

$$\alpha_{ij} = \frac{\exp\left(\mathbf{x}_i^\top \mathbf{W}_{qk} \mathbf{x}_j\right)}{\sum_j \exp\left(\mathbf{x}_i^\top \mathbf{W}_{qk} \mathbf{x}_j\right)} = \frac{\exp\left(\hat{\alpha}_{ij}\right)}{\mathcal{N}_i} \,, \tag{S12}$$

where we neglect the scaling factor $1/\sqrt{d}$ for simplicity, every $\hat{\alpha}_{ij}$ is a coefficient given by $\hat{\alpha}_{ij} = \mathbf{x}_i^\top \mathbf{W}_{qk} \mathbf{x}_j$, and $\mathcal{N}_i$ is a normalization factor defined by the row-wise softmax function $\sigma(\cdot)$ and shared across all entries in the i-th row of $\mathbf{A}$,

$$\mathcal{N}_i(\mathbf{X}; \mathbf{W}_{qk}) = \sum_j \exp\left(\mathbf{x}_i^\top \mathbf{W}_{qk} \mathbf{x}_j\right) = \sum_j \exp\left(\hat{\alpha}_{ij}\right) \,. \tag{S13}$$

The coefficients $\{\hat{\alpha}_{ij}\}$ in the second term represent the projection of $\mathbf{x}_i$ onto span$\{\mathbf{X}\}$ (the subspace spanned by $\mathbf{X} = \{\mathbf{x}_0^\top, \mathbf{x}_1^\top, \ldots, \mathbf{x}_N^\top\}$) in the transformed embedding space defined by $\mathbf{W}_{qk}$,

$$\sum_j \hat{\alpha}_{ij} \mathbf{x}_j = \sum_j \mathbf{x}_i^\top \mathbf{W}_{qk} \mathbf{x}_j \, \mathbf{x}_j = \sum_j \langle \mathbf{x}_i, \mathbf{W}_{qk} \mathbf{x}_j \rangle \, \mathbf{x}_j \,. \tag{S14}$$

It follows from the monotonically increasing property of the soft-max function that the coefficients $\{\alpha_{ij}\}$ defined in Equation (S12) preserve the order of the coefficients $\{\hat{\alpha}_{ij}\}$ while exponentially suppressing negative and near-zero values,

$$\alpha_{ij} < \alpha_{ij'} \iff \hat{\alpha}_{ij} < \hat{\alpha}_{ij'} \quad \forall i, j, j' \,. \tag{S15}$$

Therefore, the coefficients $\{\alpha_{ij}\}$ specify a convex combination that restricts the resulting vector in the convex hull Conv$(\mathbf{X}) \subset$ span$\{\mathbf{X}\}$, where the i-th row of $\mathbf{X}$ corresponding to the i-th token in the sequence is transformed into the row vector $\hat{\mathbf{x}}_i$ as follows,

$$\hat{\mathbf{x}}_i^\top = \mathbf{x}_i^\top + \sum_j \alpha_{ij} \mathbf{x}_j \mathbf{W}_v \,, \tag{S16}$$

thus concluding the proof. □

Remark S1.4. Each element of the sum in Equation (S14) implicitly defines an operator in the subspace spanned by $\mathbf{X} = \{\mathbf{x}_0^\top, \mathbf{x}_1^\top, \ldots, \mathbf{x}_N^\top\}$ given the transformed embedding space defined by $\mathbf{W}_{qk}$,

$$\sum_j \alpha_{ij}(\mathbf{W}_{qk})\, \mathbf{x}_j = \sum_j \mathbf{x}_i^\top \mathbf{W}_{qk}\mathbf{x}_j\, \mathbf{x}_j = \sum_j P_{\mathbf{W}_{qk}}(\mathbf{x}_i, \mathbf{x}_j)\,, \tag{S17}$$

where $P_{\mathbf{W}_{qk}}(\cdot, \mathbf{x}_j)$ are operators over the subset $\mathbf{X}$. The set $\mathbf{X}$ is in general linearly dependent, and the number of tokens N in the sequence differs from the embedding space dimension d. Furthermore, $\mathbf{W}_{qk}$ represents a general bilinear form (see Definition S1.2), which may not satisfy all the defining axioms of a formal inner product — namely, linearity, conjugate symmetry, and positive definiteness. Finally, the operators $P_{\mathbf{W}_{qk}}(\cdot \mathbf{x}_j)$ are not formal projection operators since they are not nilpotent ($P_{\mathbf{W}_{qk}}(\cdot \mathbf{x}_j) \circ P_{\mathbf{W}_{qk}}(\cdot \mathbf{x}_j) \neq P_{\mathbf{W}_{qk}}(\cdot \mathbf{x}_j)$). Nonetheless, the bilinear map $\mathbf{W}_{qk} : \mathbb{R}^d \times \mathbb{R}^d \to \mathbb{R}$ still associates any pair of vectors with a scalar value quantifying their alignment as determined by the geometric relations encoded in $\mathbf{W}_{qk}$. Therefore, self-attention computes a generalized decomposition of $\mathbf{x}_i$ on $\mathrm{Conv}(\mathbf{X})$ in the transformed embedding space defined by $\mathbf{W}_{qk}$. A convex combination ensures that the resulting vector remains within the region enclosed by the basis vectors $\mathbf{X}$.

Remark S1.5. Following Definition S1.1, multi-head attention consists of parallelizing the self-attention operation across H different heads with an embedding space $d_h < d$,

$$\hat{\mathbf{X}}(\mathbf{X}) = \mathbf{X} + \mathrm{concat}(\mathbf{A}_1\mathbf{V}_1, \mathbf{A}_2\mathbf{V}_2, \ldots, \mathbf{A}_h\mathbf{V}_h)\mathbf{W}_o \tag{S18}$$

where $\mathbf{A}_h = \sigma(d^{-1/2}\, \mathbf{X}\mathbf{W}_{q,h}\mathbf{W}_{k,h}^\top \mathbf{X}^T)$ is the self-attention of the h-th head, $\mathbf{W}_{q,h} \in \mathbb{R}^{d,d_h}$, $\mathbf{W}_{k,h} \in \mathbb{R}^{d,d_h}$ and $\mathbf{W}_{v,h} \in \mathbb{R}^{d,d_h}$ are the query, key, and value matrices of the h-th attention head, respectively, and $\mathbf{W}_o \in \mathbb{R}^{d,d}$ is a linear transformation [Vaswani et al., 2017]. Operationally, the self-attention computation is performed in parallel by factorizing the $\mathbf{W}_q$ and $\mathbf{W}_k$ matrices into H rectangular blocks, as follows,

$$\begin{aligned} \mathbf{W}_q &= [\mathbf{W}_{q,1}|\mathbf{W}_{q,2}|\ldots|\mathbf{W}_{q,H}] \\ \mathbf{W}_k &= [\mathbf{W}_{k,1}|\mathbf{W}_{k,2}|\ldots|\mathbf{W}_{k,H}]\,, \end{aligned} \tag{S19}$$

and performing the matrix multiplication $\mathbf{W}_{q,h}\mathbf{W}_{k,h}^\top$ per every h-th head independently in one step. It follows that the full $\mathbf{W}_{qk}$ matrix is given by the sum of the bilinear forms $\mathbf{W}_{qk,h}$ of every head, as follows,

$$\mathbf{W}_{qk} = \mathbf{W}_q\mathbf{W}_k^\top = \sum_h \mathbf{W}_{q,h}\mathbf{W}_{k,h}^\top = \sum_h \mathbf{W}_{qk,h} \tag{S20}$$

where each $\mathbf{W}_{qk,h} \in \mathbb{R}^{d,d}$ is a square matrix with $\mathrm{rank}(\mathbf{W}_{qk,h}) \leq d_h$. Therefore, each head perform independent projections onto $\mathrm{Conv}(\mathbf{X})$ that are then summed together, as follows,

$$\sum_j \hat{\alpha}_{ij}\, \mathbf{x}_j = \sum_j \mathbf{x}_i^\top \mathbf{W}_{qk}\mathbf{x}_j\, \mathbf{x}_j = \sum_j \mathbf{x}_i^\top \Big(\sum_h \mathbf{W}_{qk,h}\Big)\mathbf{x}_j\, \mathbf{x}_j = \sum_j \sum_h \langle \mathbf{x}_i, \mathbf{W}_{qk,h}\mathbf{x}_j \rangle\, \mathbf{x}_j\,, \tag{S21}$$

thus performing the same operations as in Equation (S14).

S1.3. Proof of Proposition 2.2 and related remarks

Proof. Let $U = \{t_1, \ldots, t_N\}$ be a sequence of N tokens from a vocabulary of dimension V. Let $\mathcal{L}(U)$ be the negative log-likelihood of each token t_i, expressed as

$$\mathcal{L}(U) = \sum_i \mathcal{L}(t_i) = -\sum_i \log p(t_i \,|\, \{t_j : j \in C_i\})\,, \tag{S22}$$

where $C_i \subset [0, 1, \ldots, N]$ is the set of indices defining the set of tokens $\{t_j\}$ of the conditional probability distribution. Let $\mathbf{U} = [\mathbf{t}_0, \mathbf{t}_1, \ldots, \mathbf{t}_N]$ be the sequence of N one-hot encoded tokens $\mathbf{t}_i \in \mathbb{R}^V$ associated with U, where V is the dimension of the vocabulary. Let $\mathcal{L}(\mathbf{t}_i)$ be the cross-entropy of the one-hot encoded token $\mathbf{t}_i$ and the estimated probability distribution $\sigma(\mathbf{z}_i) \in \mathbb{R}^V$, as follows,

$$\mathcal{L}(\mathbf{U}) = \sum_{i=1}^N \mathcal{L}(\mathbf{t}_i) = \sum_{i=1}^N \mathbf{t}_i \log(\sigma(\mathbf{z}_i))\,, \tag{S23}$$

15

where we let $\mathbf{z}_i$ be the prediction of the i-th token $\mathbf{t}_i$ from the representations in the last layer of a Transformer model, following Definition S1.1,

$$
\begin{cases}
\mathbf{x}_i^{0\top} = \mathbf{t_i}^\top \mathbf{W_e} + \mathbf{W}_p \\
\mathbf{x}_i^{l\top} = \mathcal{F}_l(\mathbf{x}_i^{l-1}) \quad \forall l \in [1, L] \\
\sigma(\mathbf{z}_i) = \sigma(\mathbf{x}_i^{L\top} \mathbf{W_u}),
\end{cases}
\tag{S24}
$$

where $\mathbf{x}_i^{l\top} = \mathcal{F}_l(\mathbf{x}_i^{l-1})$ is a short notation for the self-attention and multi-layered perception transformation of the l-th layer,

$$
\mathcal{F}_l(\mathbf{x}_i^{l-1}) =
\begin{cases}
\hat{\mathbf{x}}_i^{l\top} = \hat{\mathbf{x}}_i^{l-1\top} + a_l(\mathbf{x}_i^{l-1}) \\
\mathbf{x}_i^{l\top} = \hat{\mathbf{x}}_i^{l\top} + m_l(\hat{\mathbf{x}}_i^l)
\end{cases},
\tag{S25}
$$

where the self-attention function is given by

$$
a_l(\mathbf{x}_i^{l-1}) = \sum_{j \in C_i} \alpha_{ij}^l(w^l)\, \mathbf{x}_j^{l-1\top} \mathbf{W}_v^l.
\tag{S26}
$$

Let attention coefficients $\alpha_{ij}^l \equiv \alpha_{ij}^l(w^l)$ of the l-th layer be parameterized with a general parameter w^l. Let the gradient of $\mathcal{L}(\mathbf{t}_i)$ w.r.t. w_l (the parameterization of the attention scores) be factorized as follows,

$$
\nabla_{w^l} \mathcal{L}(\mathbf{t}_i) = \frac{\partial \mathcal{L}(\mathbf{t}_i)}{\partial \alpha_{ij}^l} \frac{\partial \alpha_{ij}^l}{\partial w^l}.
\tag{S27}
$$

It follows that,

$$
\begin{aligned}
\frac{\partial \mathcal{L}(\mathbf{t}_i)}{\partial \alpha_{ij}^l} &= \frac{\partial \mathcal{L}(\mathbf{t}_i)}{\partial \mathbf{z}_i} \frac{\partial \mathbf{z}_i}{\partial \mathbf{x}_i^L} \frac{\partial \mathbf{x}_i^L}{\partial \hat{\mathbf{x}}_i^l} \frac{\partial \hat{\mathbf{x}}_i^l}{\partial \alpha_{ij}^l} \\
&= (\mathbf{t}_i - \sigma(\mathbf{z}_i))^\top \mathbf{W}_u^\top \frac{\partial \mathbf{x}_i^L}{\partial \hat{\mathbf{x}}_i^l} \mathbf{W}_v^{l\top} \sum_{j \in C_i} \mathbf{x}_j^{l-1},
\end{aligned}
\tag{S28}
$$

where the term $\partial \mathbf{x}_i^L / \partial \hat{\mathbf{x}}_i^l$ includes the set of partial derivatives that define the gradient of the representation $\mathbf{x}_i^L$ at the last layer w.r.t. the self-attention representation $\hat{\mathbf{x}}_i^l$ at the l-layer, as follows,

$$
\frac{\partial \mathbf{x}_i^L}{\partial \hat{\mathbf{x}}_i^l} = \left(1 + \sum_{m=l}^{L-1} \mathcal{F}_l'(\mathbf{x}_i^m)\right)\left(1 + m_l'(\hat{\mathbf{x}}_i^l)\right),
\tag{S29}
$$

where

$$
\mathcal{F}_l'(\mathbf{x}_i^m) = \frac{\partial}{\partial \mathbf{x}_i^l} \mathcal{F}_l(\mathbf{x}_i^m) \quad ; \quad m_l'(\hat{\mathbf{x}}_i^l) = \frac{\partial}{\partial \hat{\mathbf{x}}_i^l} m_l(\hat{\mathbf{x}}_i^l).
\tag{S30}
$$

Let δ_i^l be the error at the last layer propagated to the self-attention function at the l-th layer, as follows,

$$
\delta_i^{l\top} = (\mathbf{t}_i - \sigma(\mathbf{z}_i))^\top \mathbf{W}_u^\top \frac{\partial \mathbf{x}_i^L}{\partial \hat{\mathbf{x}}_i^l} \mathbf{W}_v^{l\top},
\tag{S31}
$$

thus obtaining the following equation for the gradient,

$$
\nabla_{w^l} \mathcal{L}(\mathbf{t}_i) = \delta_i^{l\top} \sum_{j \in C_i} \mathbf{x}_j^{l-1} \frac{\partial \alpha_{ij}^l}{\partial w^l}.
\tag{S32}
$$

Let the attention scores be computed without the row-wise softmax operation and explicitly with the bilinear form $\mathbf{W}_{qk}$, such that the following expression gives the score between the i-th and jth token,

$$
\alpha_{ij}^l \equiv \alpha_{ij}^l(\mathbf{W}_{qk}^l) = \mathbf{x}_i^{l-1\top} \mathbf{W}_{qk}^l \mathbf{x}_j^{l-1},
\tag{S33}
$$

16

from which we obtain

$$\frac{\partial \alpha_{ij}^l}{\partial \mathbf{W}_{qk}^l} = \mathbf{x}_i^{l-1}\mathbf{x}_j^{l-1\top} = \mathbf{K}_{ij}^{l-1}\,, \tag{S34}$$

where $\mathbf{K}_{ij}^{l-1} \in \mathbb{M}_n$ is a square rank-1 matrix given by the outer product between the i-th and j-th token from the $l-1$-th layer. It follows that the total gradient of $\mathcal{L}(\mathbf{t}_i)$ is given by

$$\nabla_{\mathbf{W}_{qk}^l}\mathcal{L}(\mathbf{t}_i) = \delta_i^{l\top}\sum_{j\in C_i}\mathbf{x}_j^{l-1}\mathbf{K}_{ij}^{l-1}\,, \tag{S35}$$

where we notice that, for every j, the term $\delta_i^{l\top}\mathbf{x}_j^{l-1}$ is a scalar quantity that we define as β_{ij}^l, thus obtaining,

$$\nabla_{\mathbf{W}_{qk}^l}\mathcal{L}(\mathbf{t}_i) = \sum_{j\in C_i}\beta_{ij}^l\mathbf{K}_{ij}^{l-1}\,, \tag{S36}$$

and therefore,

$$\nabla_{\mathbf{W}_{qk}^l}\mathcal{L}(U) = \sum_i\sum_{j\in C_i}\beta_{ij}^l\mathbf{K}_{ij}^{l-1} \quad \forall\,\mathbf{W}_{qk}^l,\, l\in[1,L]\,. \tag{S37}$$

Equivalently, we can rewrite the double summation as follows,

$$\nabla_{\mathbf{W}_{qk}^l}\mathcal{L}(U) = \sum_{i\in P_j}\sum_j\beta_{ij}^l\mathbf{K}_{ij}^{l-1} \quad \forall\,\mathbf{W}_{qk}^l,\, l\in[1,L]\,, \tag{S38}$$

where $P_j \subset [0,1,\dots,N]$ is the set of indices defining the set of tokens $\{t_i\}$ that are predicted by t_j, thus concluding the proof. $\qquad\square$

In standard Transformer models, the bilinear form $\mathbf{W}_{qk}$ is not directly computed, and as such, it is not explicitly updated through gradient descent. Nonetheless, $\mathbf{W}_{qk}$ is implicitly updated with a combination of the weight updates of $\mathbf{W}_q$ and $\mathbf{W}_k$ having the same form as in Proposition 2.2, see the following.

Remark S1.6. Let $\mathcal{L}(\mathbf{U})$ be the negative log-likelihood of a given sequence of one-hot encoded tokens $\mathbf{U}$. Let $\mathbf{W}_q^l$ and $\mathbf{W}_k^l$ be the query and key transformation matrices of the l-th layer of Transformer models, see Definition S1.1. Let $\mathbf{W}_q^l$ and $\mathbf{W}_k^l$ be updated via gradient descent, that is, $\mathbf{W}_q^l \to \mathbf{W}_q^l + \eta\nabla_{\mathbf{W}_q^l}\mathcal{L}(\mathbf{U})$ and $\mathbf{W}_k^l \to \mathbf{W}_k^l + \eta\nabla_{\mathbf{W}_k^l}\mathcal{L}(\mathbf{U})$, where η is the learning rate. It follows that the matrix $\mathbf{W}_{qk}^l = \mathbf{W}_q^l\mathbf{W}_k^{l\top}$ is implicitly updated following,

$$\begin{aligned}
\mathbf{W}_{qk}^l &\to (\mathbf{W}_q^l + \eta\nabla_{\mathbf{W}_q^l}\mathcal{L}(U))(\mathbf{W}_k^l + \eta\nabla_{\mathbf{W}_k^l}\mathcal{L}(U))^\top \\
&= \mathbf{W}_q^l\mathbf{W}_k^{l\top} + \eta(\mathbf{W}_q^l\nabla_{\mathbf{W}_k^l}\mathcal{L}^\top(U) + \nabla_{\mathbf{W}_q^l}\mathcal{L}(U)\mathbf{W}_k^{l\top}) + o(\eta^2) \\
&= \mathbf{W}_{qk}^l + \eta\sum_i\sum_{j\in C_i}\beta_{ij}^l(\mathbf{W}_q^l\mathbf{W}_q^{l\top}\mathbf{K}_{ij}^{l-1} + \mathbf{K}_{ij}^{l-1}\mathbf{W}_k^l\mathbf{W}_k^{l\top}) + o(\eta^2) \\
&= \mathbf{W}_{qk}^l + \Delta\mathbf{W}_{qk}^l + o(\eta^2) \simeq \mathbf{W}_{qk}^l + \Delta\mathbf{W}_{qk}^l\,,
\end{aligned} \tag{S39}$$

assuming that the learning rate η is small. Therefore, the implicit weight update of $\mathbf{W}_{qk}^l$ following gradient descent is given by

$$\Delta\mathbf{W}_{qk}^l = \eta\sum_i\sum_{j\in C_i}\beta_{ij}^l\left[(\mathbf{W}_q^l\mathbf{W}_q^{l\top}\mathbf{K}_{ij}^{l-1}) + (\mathbf{K}_{ij}^{l-1}\mathbf{W}_k^l\mathbf{W}_k^{l\top})\right] \propto \sum_i\sum_{j\in C_i}\beta_{ij}^l\mathbf{K}_{ij}^{l-1}\,, \tag{S40}$$

where both $\mathbf{W}_q^l\mathbf{W}_q^{l\top}\mathbf{K}_{ij}^{l-1}$ and $\mathbf{K}_{ij}^{l-1}\mathbf{W}_k^l\mathbf{W}_k^{l\top}$ are rank-1 matrices,

$$\begin{aligned}
\mathbf{W}_q^l\mathbf{W}_q^{l\top}\mathbf{K}_{ij}^{l-1} &= \left(\mathbf{W}_q^l\mathbf{W}_q^l\mathbf{x}_i^{l-1}\right)\mathbf{x}_j^{l-1\top} = \bar{\mathbf{x}}_i^{l-1}\mathbf{x}_j^{l-1\top} \\
\mathbf{K}_{ij}^{l-1}\mathbf{W}_k^l\mathbf{W}_k^{l\top} &= \mathbf{x}_i^{l-1}\left(\mathbf{x}_j^{l-1\top}\mathbf{W}_k^l\mathbf{W}_k^{l\top}\right) = \mathbf{x}_i^{l-1}\bar{\mathbf{x}}_j^{l-1\top}\,.
\end{aligned} \tag{S41}$$

S1.4. Formal proofs for the connection between objective functions, directionality, and symmetry

In this section, we provide a formal mathematical derivation of the informal Theorems 2.3 and 2.4 introduced in the main text. To do so, we provide a formal description and proof of the Theorems for the directionality and symmetric structures during autoregressive and bidirectional training, respectively with Theorem S1.12 and Theorem S1.14. We also introduce a series of related Propositions and Lemmas.

S1.4.1 Different implicit update of rows and columns

First, we show that a token t^* contributes differently to the updates of $\mathbf{W}_{qk}$ depending on whether it serves as context for predicting other tokens or is itself predicted. When t^* is used to predict a set of tokens:

- All predicted tokens contribute to the column space of $\mathbf{W}_{qk}$ with the update of the k-th column scaled by the associated entry $[\mathbf{x}_{t^*}]_k$.
- Only the token t^* contributes to the row space, with the update to the m-th row scaled a linear combination of $[\mathbf{x}_i]_m$ for all predicted tokens.

On the other hand, when t^* is predicted by a set of tokens:

- Only the token t^* contributes to the column space, with the update to the k-th row scaled a linear combination of $[\mathbf{x}_i]_k$ for all predicted tokens.
- All context tokens contribute to the row space with the update of the m-th column scaled by the associated entry $[\mathbf{x}_{t^*}]_m$.

We formalize this in the following Proposition.

Proposition S1.7. *(Different implicit updates for context and prediction). Let $U = [t_0, \dots, t_N]$ be a sequence of tokens and let $\mathbf{x}_i \in \mathbb{R}^d$ be the embedding of the i-th token. Let $\Delta\mathbf{W}_{qk}$ be the weight update from Proposition 2.2. Let t^* be a given token in U. When using t^* as context, the k-th column of $\Delta\mathbf{W}_{qk}$ is given by*

$$\Delta\mathbf{w}_{\cdot,k}\bigg|_{t_j=t^*} = [\mathbf{x}_{t^*}]_k \left(\sum_{i \in P_{t^*}} \beta_{ij}\mathbf{x}_i \right), \tag{S42}$$

while the m-th row of $\Delta\mathbf{W}_{qk}$ is given by

$$\Delta\mathbf{w}_{m,\cdot}\bigg|_{t_j=t^*} = \left(\sum_{i \in P_{t^*}} \beta_{ij}[\mathbf{x}_i]_m \right) \mathbf{x}_{t^*}, \tag{S43}$$

where P_{t^*} is the set of tokens predicted by t^*. When predicting t^*, the k-th column of $\Delta\mathbf{W}_{qk}$ is given by

$$\Delta\mathbf{w}_{k,\cdot}\bigg|_{t_i=t^*} = \left(\sum_{j \in C_{t^*}} \beta_{t^*j}[\mathbf{x}_j]_k \right) \mathbf{x}_{t^*}, \tag{S44}$$

while the m-th row of $\Delta\mathbf{W}_{qk}$ is given by

$$\Delta\mathbf{w}_{m,\cdot}\bigg|_{t_i=t^*} = [\mathbf{x}_{t^*}]_m \left(\sum_{j \in C_{t^*}} \beta_{t^*j}\mathbf{x}_j^\top \right). \tag{S45}$$

where C_{t^*} is the set of context tokens for t^*.

Proof. Let $\mathbf{U} = [t_0, \dots, t_N]$ a sequence of tokens with the embedding of every i-th token be given by $\mathbf{x}_i \in \mathbb{R}^d$. The implicit weight update of Proposition 2.2 can be decomposed with two equivalent regrouping of the double summations, as follows,

$$\Delta\mathbf{W}_{qk} = \sum_{(i,j)\in\mathbf{U}} \beta_{ij}\mathbf{x}_i\mathbf{x}_j^T = \sum_j \left(\sum_{i\in P_j} \beta_{ij}\mathbf{x}_i \right) \mathbf{x}_j^\top = \sum_i \mathbf{x}_i \left(\sum_{i\in C_i} \beta_{ij}\mathbf{x}_j^\top \right), \tag{S46}$$

18

where $P_i \subset U$ is the set of tokens predicted by a given token t_i, while $C_j \subset U$ is the set of tokens that predict a given token t_j. We neglect any constant of proportionality - such as a learning rate - for simplicity. For simplicity, we do not assume any specific structure on P_i and C_j (autoregressive training, bidirectional training, or others). First, the contribution of $t^* \in U$ to the weight update when t^* is used as context to predict a set of tokens $P_{t^*} \subset U$ is

$$\Delta \mathbf{W}_{qk}\Big|_{t_j=t^*} = \left(\sum_{i \in P_{t^*}} \beta_{it^*} \mathbf{x}_i \right) \mathbf{x}_{t^*}^\top . \tag{S47}$$

The associated weight update of the k-th column is then given by

$$\Delta \mathbf{w}_{\cdot,k}\Big|_{t_j=t^*} = \left(\sum_{i \in P_{t^*}} \beta_{it^*} \mathbf{x}_i \right) [\mathbf{x}_{t^*}]_k = [\mathbf{x}_{t^*}]_k \left(\sum_{i \in P_{t^*}} \beta_{it^*} \mathbf{x}_i \right) , \tag{S48}$$

while the update of the m-th row is

$$\Delta \mathbf{w}_{m,\cdot}\Big|_{t_j=t^*} = \left(\sum_{i \in P_{t^*}} \beta_{it^*} [\mathbf{x}_i]_m \right) \mathbf{x}_{t^*} . \tag{S49}$$

A complementary argument can be made when predicting a given token t^* from a set of tokens C_{t^*}. Indeed, the contribution to the weight update when t^* is predicted by set of tokens $C_{t^*} \subset U$ is given by

$$\Delta \mathbf{W}_{qk}\Big|_{t_i=t^*} = \left(\sum_{j \in C_{t^*}} \beta_{t^* j} \mathbf{x}_{t^*} \right) \mathbf{x}_j^\top . \tag{S50}$$

The associated weight update of the k-th column is then given by

$$\Delta \mathbf{w}_{k,\cdot}\Big|_{t_i=t^*} = \left(\sum_{j \in C_{t^*}} \beta_{t^* j} [\mathbf{x}_j]_k \right) \mathbf{x}_{t^*} , \tag{S51}$$

while the update of the m-th row is

$$\Delta \mathbf{w}_{m,\cdot}\Big|_{t_i=t^*} = \left(\sum_{j \in C_{t^*}} \beta_{t^* j} \mathbf{x}_j^\top \right) [\mathbf{x}_{t^*}]_m = [\mathbf{x}_{t^*}]_m \left(\sum_{j \in C_{t^*}} \beta_{t^* j} \mathbf{x}_j^\top \right) . \tag{S52}$$

Therefore, the weight update of each column (row) when a set of tokens predicts t^* is equivalent to the weight update of each row (column) when t^* is used to predict a set of tokens. This concludes the proof. □

S1.4.2   Asymmetric growth of rows and columns during weight update

Next, we demonstrate that under reasonable assumptions about the statistical distribution of token embeddings, the expected norm of column updates exceeds that of row updates when using the token t^* to predict other tokens. Conversely, when t^* is being predicted by other tokens, the row updates become dominant. We begin by assuming that the token embeddings $\mathbf{x}_i$ are independent and identically distributed (i.i.d.) random vectors drawn from a probability distribution $\mathcal{D}$ with zero mean, $\mathbb{E}[\mathbf{x}_i] = \mathbf{0}$, and covariance matrix $\mathrm{Cov}(\mathbf{x}_i) = \Sigma$. This assumption holds true at initialization for any Transformer model with learnable embeddings. Additionally, we assume that the covariance matrix satisfies $\Sigma \neq \sigma^2 \mathbb{I},$. More specifically, we posit that there is partial alignment between the embeddings $\mathbf{x}_i$ due to the semantic and predictive relationships between tokens, which typically emerge in the vector embeddings during training. Similar to Proposition S1.7, the scenarios where t^* is used to predict other tokens and where t^* is being predicted by other tokens are complementary. In the following Proposition, we focus solely on the case where t^* serves as context to predict a set of tokens. A formal derivation for the opposite case where t^* is predicted by other tokens is provided in a subsequent Corollary.

19

Proposition S1.8. (*Asymmetric growth of columns and rows for context*). *Let $U = [t_0, \ldots, t_N]$ a sequence of tokens, and let t^* be a token representing the context of every token $t_i \in U$. Let $\{\mathbf{x}_1 \ldots, \mathbf{x}_N\}$ be the token embedding associated with U such that each $\mathbf{x}_i \sim \mathcal{D}$ is a i.i.d. random vector drawn from a probability distribution $\mathcal{D}$ with zero mean and non-isotropic covariance $Cov(\mathbf{x}_i) = \Sigma$. Let $\mathbf{y}$ be the independent random embedding of t^* with zero mean and covariance $Cov(\mathbf{y}) = \sigma_y^2 \mathbb{I}$. Let $\Delta \mathbf{W}_{qk}$ be the weight update from Proposition 2.2. Then the squared norm of the m-th row and k-th column of $\mathbf{W}_{qk}$ satisfies*

$$\frac{\mathbb{E}\left[\|\Delta \mathbf{w}_{\cdot,k}\|^2\right]}{\mathbb{E}\left[\|\Delta \mathbf{w}_{m,\cdot}\|^2\right]} > 1 \quad \forall k \in \{1, \ldots, d\}, \forall m \text{ s.t. } \Sigma_{m,m} < \frac{Tr(\Sigma)}{d} \tag{S53}$$

Proof. Let $U = [t_0, \ldots, t_N]$ a sequence of tokens, and let t^* be the context of every token $t_i \in U$. Let $\{\mathbf{x}_i\}$ be the set of token embeddings associated with U and let $\mathbf{y}$ be the token embedding of t^*. It follows from Proposition S1.7 that the squared norm of the weight update of the k-th column is given by

$$\Delta \mathbf{w}_{\cdot,k} = \sum_{j \in \{t^*\}} \sum_{i \in P_j} \beta_{ij} \mathbf{x}_i [\mathbf{x_j}]_k = \sum_{i=1}^{N} \beta_{it^*} \mathbf{x}_i [\mathbf{y}]_k \Rightarrow \|\Delta \mathbf{w}_{\cdot,k}\|^2 = [\mathbf{y}]_k^2 \| \sum_{i=1}^{N} \beta_{it^*} \mathbf{x}_i\|^2, \tag{S54}$$

while the squared norm of the weight update of the m-th row by

$$\Delta \mathbf{w}_{m,\cdot} = \sum_{j \in \{t^*\}} \sum_{i \in P_j} \beta_{it^*} [\mathbf{x}_i]_m \mathbf{x}_j = \sum_{i=1}^{N} \beta_{it^*} [\mathbf{x}_i]_m \mathbf{y} \Rightarrow \|\Delta \mathbf{w}_{m,\cdot}\|^2 = (\sum_{i=1}^{N} \beta_{it^*} [\mathbf{x}_i]_m)^2 \|\mathbf{y}\|^2. \tag{S55}$$

Let $\{\mathbf{x}_i\} \sim \mathcal{D}$ be a set of i.i.d. random vectors from a probability distribution $\mathcal{D}$ such that $\mathbb{E}[\mathbf{x}_i] = 0$ and $Cov(\mathbf{x}_i) = \Sigma \in \mathbb{R}^{d,d}$. Therefore, each k-th coordinate $[\mathbf{x}_i]_k$ is such that $\mathbb{E}[[\mathbf{x}_i]_k] = 0$ and $Var([\mathbf{x}_i]_k) = \Sigma_{k,k}$. We also assume that $\mathbf{y}$ is statistically independent from $\mathbf{x}_i \forall i$ with $\mathbb{E}[\mathbf{y}] = 0$ and covariance $Cov(\mathbf{y}) = \sigma_y^2 \mathbb{I}$. It follows that the expected value of $\|\Delta \mathbf{w}_{\cdot,k}\|^2$ over $\mathcal{D}$ is given by

$$\mathbb{E}\left[\|\Delta \mathbf{w}_{\cdot,k}\|^2\right] = \mathbb{E}\left[[\mathbf{y}]_k^2 \| \sum_{i=1}^{N} \beta_{it^*} \mathbf{x}_i\|^2\right] = \mathbb{E}\left[[\mathbf{y}]_k^2\right] \mathbb{E}\left[\| \sum_{i=1}^{N} \beta_{it^*} \mathbf{x}_i\|^2\right]. \tag{S56}$$

Given the statistical independence between the entries of $\mathbf{x}_i$, the second term is equal to

$$\begin{aligned} \mathbb{E}\left[\| \sum_{i=1}^{N} \beta_{it^*} \mathbf{x}_i\|^2\right] &= \sum_{i,i'} \mathbb{E}\left[\beta_{it^*} \beta_{i't^*} \mathbf{x}_i^\top \mathbf{x}_{i'}\right] \\ &= \sum_{i} \beta_{it^*}^2 \mathbb{E}\left[\mathbf{x}_i^\top \mathbf{x}_i\right] + \sum_{i' \neq i} \beta_{it^*} \beta_{i't^*} \mathbb{E}\left[\mathbf{x}_i^\top \mathbf{x}_{i'}\right] \\ &= \sum_{i} \beta_{it^*}^2 Tr(\mathbb{E}\left[\mathbf{x}_i \mathbf{x}_i^\top\right]) + \sum_{i' \neq i} \beta_{it^*} \beta_{i't^*} \mathbb{E}\left[\mathbf{x}_i^\top \mathbf{x}_{i'}\right] \\ &= Tr(\Sigma) \sum_{i} \beta_{it^*}^2, \end{aligned} \tag{S57}$$

and therefore

$$\mathbb{E}\left[\|\Delta \mathbf{w}_{\cdot,k}\|^2\right] = \Gamma_{k,k} Tr(\Sigma) \sum_{i} \beta_{it^*}^2. \tag{S58}$$

Similarly, the expected value of $\|\Delta \mathbf{w}_{m,\cdot}\|^2$ is given by

$$\mathbb{E}\left[\|\Delta \mathbf{w}_{m,\cdot}\|^2\right] = \mathbb{E}\left[(\sum_{i=1}^{N} \beta_{it^*} [\mathbf{x}_i]_m)^2 \|\mathbf{y}\|^2\right] = \mathbb{E}\left[(\sum_{i=1}^{N} \beta_{it^*} [\mathbf{x}_i]_m)^2\right] \mathbb{E}\left[\|\mathbf{y}\|^2\right]. \tag{S59}$$

The first term can be decomposed as

$$\mathbb{E}\left[(\sum_{i=1}^{n} \beta_{it^*} [\mathbf{x}_i]_m)^2\right] = \sum_{i=1}^{n} \beta_{it^*}^2 \mathbb{E}\left[[\mathbf{x}_i]_m^2\right] + \sum_{i' \neq i} \beta_{it^*} \beta_{i't^*} \mathbb{E}\left[[\mathbf{x}_{i'}]_m [\mathbf{x}_i]_m\right] = \Sigma_{m,m} \sum_{i=1}^{n} \beta_{it^*}^2, \tag{S60}$$

20

and therefore

$$\mathbb{E}\left[\|\Delta\mathbf{w}_{m,\cdot}\|^2\right] = \Sigma_{m,m}\mathrm{Tr}(\Gamma)\sum_i \beta_{it^*}^2 . \tag{S61}$$

The ratio of the expected value of these squared norms is

$$\frac{\mathbb{E}\left[\|\Delta\mathbf{w}_{\cdot,k}\|^2\right]}{\mathbb{E}\left[\|\Delta\mathbf{w}_{m,\cdot}\|^2\right]} = \frac{\Gamma_{k,k}\mathrm{Tr}(\Sigma)}{\Sigma_{m,m}\mathrm{Tr}(\Gamma)} = \frac{\Gamma_{k,k}}{\mathrm{Tr}(\Gamma)}\frac{\mathrm{Tr}(\Sigma)}{\Sigma_{m,m}} = \frac{1}{d}\frac{\mathrm{Tr}(\Sigma)}{\Sigma_{m,m}} . \tag{S62}$$

We assume a non-isotropic covariance structure in Σ, that is, the average variance per dimension is lower than the total variance across all dimensions. This implies $\mathrm{Tr}(\Sigma) > d\,\Sigma_{m,m}$ for some m. It follows that,

$$\frac{\mathbb{E}\left[\|\Delta\mathbf{w}_{\cdot,k}\|^2\right]}{\mathbb{E}\left[\|\Delta\mathbf{w}_{m,\cdot}\|^2\right]} = \frac{1}{d}\frac{\mathrm{Tr}(\Sigma)}{\Sigma_{m,m}} > \frac{1}{d}\frac{d\,\Sigma_{m,m}}{\Sigma_{m,m}} = 1 \quad \forall m \text{ s.t. } \Sigma_{m,m} < \frac{\mathrm{Tr}(\Sigma)}{d} , \tag{S63}$$

thus concluding the proof. $\qquad\square$

Again, a complementary argument on asymmetric weight update can be made when a set of tokens $U = \{t_1, \ldots, t_N\}$ is used to predict a given token t^*, that is, $C_i = \{t^*\}\ \forall t_i \in U$. We formalize this in the following Corollary.

Corollary S1.9. *(Asymmetric growth of columns and rows for prediction). Let $U = [t_0, \ldots, t_N]$ a sequence of tokens, and let every token $t_i \in U$ be the context of a given token t^*. Let the associated embedding be drawn i.i.d. from a probability distribution $\mathcal{D}$ as in Proposition S1.8. Let $\Delta\mathbf{W}_{qk}$ be the weight update from Proposition 2.2. Then the squared norm of the m-th row and k-th column of $\mathbf{W}_{qk}$ satisfies*

$$\frac{\mathbb{E}\left[\|\Delta\mathbf{w}_{\cdot,k}\|^2\right]}{\mathbb{E}\left[\|\Delta\mathbf{w}_{m,\cdot}\|^2\right]} < 1 \quad \forall m \in \{1, \ldots, d\}, \forall k \text{ s.t. } \Sigma_{k,k} < \frac{Tr(\Sigma)}{d} \tag{S64}$$

Proof. Let $U = [t_0, \ldots, t_N]$ a sequence of tokens, and let t^* be predicted by every token $t_i \in U$. Let $\{\mathbf{x}_i\}$ be the set of token embeddings associated with U and let $\mathbf{y}$ be the token embedding of t^*. It follows from Proposition S1.7 that the squared norm of the weight update of the k-th column is given by

$$\Delta\mathbf{w}_{\cdot,k} = \sum_{i=\{t^*\}}\sum_{j\in C_i}[\mathbf{x}_j]_k\mathbf{x}_i = \sum_{j=1}^N[\mathbf{x}_j]_k\mathbf{y} \;\Rightarrow\; \|\Delta\mathbf{w}_{\cdot,k}\|^2 = \Big(\sum_{i=1}^N[\mathbf{x}_j]_k\Big)^2\|\mathbf{y}\|^2 , \tag{S65}$$

while the weight update of the m-th row follows

$$\Delta\mathbf{w}_{m,\cdot} = \sum_{i=\{t^*\}}\sum_{j\in C_i}\mathbf{x}_j[\mathbf{x_i}]_m = \sum_{j=1}^N\mathbf{x}_j[\mathbf{y}]_m \;\Rightarrow\; \|\Delta\mathbf{w}_{m,\cdot}\|^2 = [\mathbf{y}]_m^2\|\sum_{i=1}^N\mathbf{x}_j\|^2 . \tag{S66}$$

Therefore, following the same arguments as in Proposition S1.4.2, the ratio of the expected value of the square norms is given by

$$\frac{\mathbb{E}\left[\|\Delta\mathbf{w}_{\cdot,k}\|^2\right]}{\mathbb{E}\left[\|\Delta\mathbf{w}_{m,\cdot}\|^2\right]} = \frac{\Sigma_{k,k}\mathrm{Tr}(\Gamma)}{\Gamma_{m,m}\mathrm{Tr}(\Sigma)} = d\frac{\Sigma_{k,k}}{\mathrm{Tr}(\Sigma)} < \frac{d\,\Sigma_{k,k}}{d\,\Sigma_{k,k}} = 1 \quad \forall k \text{ s.t. } \Sigma_{k,k} < \frac{\mathrm{Tr}(\Sigma)}{d} , \tag{S67}$$

thus concluding the proof. $\qquad\square$

S1.4.3 Average contribution of a given token for context and prediction

Additionally, we demonstrate that during autoregressive training, the expected number of tokens predicted by a specific token t^* can differ from the expected number of tokens that predict t^*. More specifically, in autoregressive training, the ratio between these two expected numbers is influenced by the statistical correlations between tokens in the dataset. In contrast, for bidirectional training, the expected number of tokens predicted by t^* and the number of tokens that predict t^* are always equal. This equality holds true regardless of how tokens are correlated within the corpus, resulting in a ratio of 1. We formalize this in the following Proposition.

21

Proposition S1.10. *Let $\mathcal{V} = [t_0, \ldots, t_V]$ be a set of tokens. Let $\mathcal{U}$ be the sample space of all possible sequences of N tokens, and let $U \in \mathcal{U}$ be a sequence $U = [t_1, \ldots, t_N]$. Let $\Pr[t_j = t^*]$ be the probability that the token at index j in is given by $t^* \in \mathcal{V}$. Let $\mathbb{E}[\mu_c(t^*)]$ be the expected number of tokens that are predicted by a given token t^*, and $\mathbb{E}[\mu_p(t^*)]$ the expected number of tokens that predict a given token t^*. For autoregressive training, the ratio*

$$\frac{\mathbb{E}[\mu_c(t^*)]}{\mathbb{E}[\mu_p(t^*)]} = \frac{\sum_{k=1}^{N}(N-k)\Pr[t_k = t^*]}{\sum_{k=1}^{N}(k-1)\Pr[t_k = t^*]}, \tag{S68}$$

depends on $\Pr[t_j = t^*]$, while for bidirectional training the same ratio is given by

$$\frac{\mathbb{E}[\mu_c(t^*)]}{\mathbb{E}[\mu_p(t^*)]} = 1. \tag{S69}$$

Proof. Let $\mathcal{V} = [t_0, \ldots, t_V]$ be a set of tokens. Let $\mathcal{U}$ be the sample space of all possible sequences of N tokens, and let U be a sequence $U = [t_1, \ldots, t_N] \in \mathcal{U}$. Let $E = \{U \in \mathcal{U} : t_k = t^*\}$ the event of all sequences where the k-th token is t^*. The indicator function $\mathbb{1}\{E\}(U)$ is a random variable defined as

$$\mathbb{1}\{E\}(U) = \begin{cases} 1 \text{ if } t_k = t^* \\ 0 \text{ otherwise}, \end{cases} \tag{S70}$$

and as such its expected value over $\mathcal{U}$ is

$$\mathbb{E}\left[\mathbb{1}\{t_k = t^*\}(U)\right] = \sum_{U \in \mathcal{U}} \mathbb{1}\{t_k = t^*\}(U)\Pr[U] = \sum_{U \in \mathcal{U} : w_j = t^*} \Pr[U] = \Pr[t_k = t^*]. \tag{S71}$$

Let $\mu_c(t^*)$ be the random variable quantifying the number of tokens predicted by t^*, while $\mu_p(t^*)$ is the random variable quantifying the number of tokens predicted by t^*. We analyzed the case of autoregressive and bidirectional training separately.

During autoregressive training, each time the token t^* appears at position k it is used as context to predict $N - k$ tokens, and it is predicted by $k - 1$ tokens. It follows that $\mu_c(t^*)$ is given by

$$\mu_c(t^*) = \sum_{l=2}^{N}\sum_{k=1}^{l-1}\mathbb{1}\{t_k = t^*\} = \sum_{k=1}^{N}(N-k)\mathbb{1}\{t_k = t^*\}, \tag{S72}$$

while $\mu_p(t^*)$ is given by

$$\mu_p(t^*) = \sum_{l=1}^{N-1}\sum_{k=1}^{l-1}\mathbb{1}\{t_l = t^*\} = \sum_{k=1}^{N}(k-1)\mathbb{1}\{t_k = t^*\}. \tag{S73}$$

Therefore, the expected value of $\mu_c(t^*)$ over all possible sequences is

$$\mathbb{E}[\mu_c(t^*)] = \mathbb{E}\left[\sum_{k=0}^{N}(N-k)\mathbb{1}\{t_k = t^*\}\right] = \sum_{k=0}^{N}(N-k)\Pr[t_k = t^*], \tag{S74}$$

the expected value of $\mu_p(t^*)$ is

$$\mathbb{E}[\mu_p(t^*)] = \mathbb{E}\left[\sum_{k=0}^{N}(k-1)\mathbb{1}\{t_k = t^*\}\right] = \sum_{k=0}^{N}(k-1)\Pr[t_k = t^*], \tag{S75}$$

and their ratio is given by

$$\frac{\mathbb{E}[\mu_c(t^*)]}{\mathbb{E}[\mu_p(t^*)]} = \frac{\sum_{k=1}^{N}(N-k)\Pr[t_k = t^*]}{\sum_{k=1}^{N}(k-1)\Pr[t_k = t^*]}. \tag{S76}$$

During bidirectional training, each time the token t^* is masked at position k, it is predicted by $N - 1$ tokens. We assume that the token t^* significantly contributes to the context of a masked token only if it is itself not

masked. During bidirectional training, whenever a token t^* at position k is masked, it is predicted using the other $N - 1$ tokens in the sequence. We assume that t^* significantly contributes to the context for predicting the masked token only if t^* itself is not masked. Additionally, we assume that the probability ρ of masking any given position k is the same for all positions and does not depend on the specific token t_k at that position. It follows that $\mu_c(t^*)$ is given by

$$\mu_c(t^*) = \sum_{k=1}^{N} \mathbb{1}\{t_k = t^*\}\mathbb{1}\{\text{mask}(k) = 0\} \sum_{k' \neq k} \mathbb{1}\{\text{mask}(k') = 1\}, \tag{S77}$$

while $\mu_p(t^*)$ is given by

$$\mu_p(t^*) = \sum_{k=1}^{N} \mathbb{1}\{t_k = t^*\}\mathbb{1}\{\text{mask}(k) = 1\} \sum_{k' \neq k} \mathbb{1}\{\text{mask}(k') = 0\}. \tag{S78}$$

Therefore, their expected values are given by

$$\begin{aligned}
\mathbb{E}[\mu_c(t^*)] &= \mathbb{E}\left[\sum_{k=1}^{N} \mathbb{1}\{t_k = t^*\}\mathbb{1}\{\text{mask}(k) = 0\} \sum_{k' \neq k} \mathbb{1}\{\text{mask}(k') = 1\}\right] \\
&= \sum_{k=1}^{N} \mathbb{E}\left[\mathbb{1}\{t_k = t^*\}\mathbb{1}\{\text{mask}(k) = 0\} \sum_{k' \neq k} \mathbb{1}\{\text{mask}(k') = 1\}\right] \\
&= \sum_{k=1}^{N} \mathbb{E}\left[\mathbb{1}\{t_k = t^*\}\mathbb{1}\{\text{mask}(k) = 0\}\right] \sum_{k' \neq k} \left[\mathbb{1}\{\text{mask}(k') = 1\}\right] \\
&= \sum_{k=1}^{N} \Pr(t_k = t^*)\Pr(\text{mask}(k) = 0) \sum_{k' \neq k} \Pr(\text{mask}(k') = 1) \\
&= N\rho(N - 1)(1 - \rho) \sum_{k=1}^{N} \Pr(t_k = t^*),
\end{aligned} \tag{S79}$$

and

$$\begin{aligned}
\mathbb{E}[\mu_p(t^*)] &= \mathbb{E}\left[\sum_{k=1}^{N} \mathbb{1}\{t_k = t^*\}\mathbb{1}\{\text{mask}(k) = 1\} \sum_{k' \neq k} \mathbb{1}\{\text{mask}(k') = 0\}\right] \\
&= N\rho(N - 1)(1 - \rho) \sum_{k=1}^{N} \Pr(t_k = t^*),
\end{aligned} \tag{S80}$$

and their ratio is

$$\frac{\mathbb{E}[\mu_c(t^*)]}{\mathbb{E}[\mu_p(t^*)]} = 1, \tag{S81}$$

thus concluding the proof.

$\square$

Let us assume that there is no statistical correlation between the tokens in U, we can factorize the joint probability $\Pr[U]$ as follows

$$\Pr[U] = \Pr[t_1, \ldots, t_N] = \Pi_{i=1}^{N} \Pr[t_i]. \tag{S82}$$

Additionally, let us assume that each token is identically distributed independently of the position. Therefore, during autoregressive training, the expected number $\mathbb{E}[\mu_c(t^*)]$ can be simplified as

$$\mathbb{E}[\mu_c(t^*)] = \sum_{k=0}^{N} (N - k) \Pr[t_k = t^*] = \sum_{k=0}^{N} (N - k) \Pr[t^*] = \Pr[t^*]\frac{N(N - 1)}{2}, \tag{S83}$$

and the same is true for $\mathbb{E}[\mu_p(t^*)]$

$$\mathbb{E}[\mu_p(t^*)] = \sum_{k=0}^{N}(k-1)\Pr[t_k = t^*] = \sum_{k=0}^{N}(k-1)\Pr[t^*] = \Pr[t^*]\frac{N(N-1)}{2}. \qquad (S84)$$

It follows that, in the case of statistical independence between tokens, the expected number of tokens predicted by t^* and the expected number of tokens predicting t^*. Under these assumptions, there is no difference between autoregressive and bidirectional training.

On the other hand, let us assume a general joint probability between tokens, $\Pr[U] = \Pr[t_1, \ldots, t_N]$. When conditioning the probabilities over the future tokens, we obtain a factorization of the joint probability as follows,

$$\Pr[U] = \prod_{i=1}^{N}\Pr[t_i \mid t_{i+1}, \ldots, t_N]. \qquad (S85)$$

The probability of the k-th token being t^* across the possible sequences is thus given by

$$\Pr[t_k = t^*] = \sum_{t_1, \ldots, t_N} \mathbb{1}\{t_k = t^*\}\Pr[t_1, \ldots, t_n]$$

$$= \sum_{t_1, \ldots, t_{k-1}, t_{k+1}, \ldots, t_N} \left(\prod_{\substack{l=1 \\ l \neq k}}^{T}\Pr[t_l|t_{l+1}, \ldots, t_N]\right) \cdot \Pr[t_k = t|t_{k+1}, \ldots, t_N], \qquad (S86)$$

leading to the ratio

$$\frac{\mathbb{E}[\mu_c(t^*)]}{\mathbb{E}[\mu_p(t^*)]} = \frac{\sum_{k=1}^{N}(N-k)\sum_{t_1, \ldots, t_{k-1}, t_{k+1}, \ldots, t_N}\left(\prod_{\substack{l=1 \\ l \neq k}}^{T}\Pr[t_l|t_{l+1}, \ldots, t_N]\right)\cdot\Pr[t_k = t|t_{k+1}, \ldots, t_N]}{\sum_{k=1}^{N}(k-1)\sum_{t_1, \ldots, t_{k-1}, t_{k+1}, \ldots, t_N}\left(\prod_{\substack{l=1 \\ l \neq k}}^{T}\Pr[t_l|t_{l+1}, \ldots, t_N]\right)\cdot\Pr[t_k = t|t_{k+1}, \ldots, t_N]}. \qquad (S87)$$

Therefore, when t^* has a high probability of occurring before a given set of tokens, or when t^* is likely to occur at the beginning of sentences and specific pieces of text, this ratio is likely to be higher than 1.

S1.4.4 Theorem on the emergence of directionality

Here, we show that, under the same assumptions as in Proposition S1.8, the weight updates of $\mathbf{W}_{qk}$ induce column dominance during autoregressive training. Specifically, there are on average more columns with high norms than rows with high norms. We assume that, at initialization, the entries of $\mathbf{W}_{qk}$ are drawn from a probability distribution $\mathcal{P}$ with finite mean μ and variance σ^2. This assumption holds for any standard machine learning initialization scheme. This implies that each k-th column $\mathbf{w}_{\cdot,k}$ and m-th row $\mathbf{w}_{m,\cdot}$ have the same mean μ and variance $\sigma^2/\sqrt{n}$. Furthermore, the squared norm of both rows and columns have equal mean $n(\sigma^2 + \mu^2)$ and variance $n(2\sigma^4 + 4\mu^2)$.

To demonstrate the column dominance, we first show that if one probability distribution has a higher variance than another, it is more likely to produce samples with higher values. We formalize this in the following Lemma.

Lemma S1.11. *Let two probability distributions a, b have the same mean μ and different variance $\sigma_a^2 > \sigma_b^2$. The probability of a random sample of each distribution being larger than a value z is higher for samples from a than from b for $z > \sqrt{\sigma_a \sigma_b} - \mu$,*

$$Pr[X_a > z] \geq Pr[X_b > z] \quad \forall z > \sqrt{\sigma_a \sigma_b} - \mu \qquad (S88)$$

Proof. Our goal is to find a z such that

$$Pr[X_a > z] \geq Pr[X_b > z] \qquad (S89)$$

24

for which we need the following steps: A lower bound for $\Pr[X_a > z]$, an upper bound for $\Pr[X_b > z]$, and a value of z that makes the upper bound lower than the lower bound.

We start by using Chebyshev's inequality, to derive an upper bound for $\Pr[X_b > z]$,

$$\Pr[X_b > z] = \Pr[X_b - \mu > q\sigma_b] \leq \frac{1}{q^2} = \left(\frac{\sigma_b}{z - \mu}\right)^2. \tag{S90}$$

Now compute a lower bound for $\Pr[X_b > z]$ through the second moment method (which is very similar to the previous one, but inverted),

$$\Pr[X_a > z] = \Pr[X_a - z > 0] \geq \frac{(\mathbb{E}[X_a - z])^2}{\mathbb{E}\left[(X_a - z)^2\right]} = \left(\frac{\mu - z}{\sigma_a}\right)^2 \tag{S91}$$

Thus, we now only need to find z satisfying

$$\left(\frac{\sigma_b}{z - \mu}\right)^2 < \left(\frac{z - \mu}{\sigma_a}\right)^2 \tag{S92}$$

for the case $z > \mu$, the inequality is fulfilled when

$$z > \sqrt{\sigma_a \sigma_b} - \mu. \tag{S93}$$

$\square$

We now formalize the connection between this result and the asymmetric growth of columns in the following Theorem.

Theorem S1.12. (*Autoregressive training induces directionality*) *Let $\mathcal{V} = [t_0, \ldots, t_V]$ be a set of tokens. Let U be an ordered sequence of N tokens $U = [t_1, \ldots, t_N]$ where $\Pr[t_j = t^*]$ is the probability that the token at index j in U is given by $t^* \in \mathcal{V}$. Let $\{\mathbf{x}_1 \ldots, \mathbf{x}_n\}$ be the embedding associated with $\mathcal{V}$ such that each $\mathbf{x}_i \sim \mathcal{D}$ is drawn i.i.d. from a probability distribution $\mathcal{D}$ with zero mean and semipositive covariance $Cov(\mathbf{x}_i) \neq \sigma_x^2 \mathbb{I}$. Let $\Delta\mathbf{W}_{qk}$ be the weight update of $\mathbf{W}_{qk}$ from Proposition 2.2. Let $\Delta\mathbf{W}_{qk}$ be derived from an autoregressive objective function as in Definition S1.3. Then, there exists a value $\gamma \in \mathbb{R}$ such that,*

$$Pr[\|\mathbf{w}_{\cdot,k}\| > w] > Pr[\|\mathbf{w}_{m,\cdot}\| > w] \quad \forall \, w > \gamma \tag{S94}$$

Proof. Let $\mathbb{E}[\mu_c(t^*)]$ be the expected number of tokens that are predicted by a given token t^*, and $\mathbb{E}[\mu_p(t^*)]$ the expected number of tokens that predict a given token t^*. When assuming autoregressive training, it follows from Proposition S1.10 that

$$\frac{\mathbb{E}[\mu_c(t^*)]}{\mathbb{E}[\mu_p(t^*)]} = \frac{\sum_{j=1}^{N}(N - j)\Pr[t_j = t^*]}{\sum_{j=1}^{N}(j - 1)\Pr[t_j = t^*]}. \tag{S95}$$

Let the statistical correlation between tokens in U,

$$\frac{\mathbb{E}[\mu_c(t^*)]}{\mathbb{E}[\mu_p(t^*)]} > 1, \tag{S96}$$

for most $t^* \in \mathcal{V}$. It follows that the average number of tokens that are predicted by t^* is smaller than the average number of tokens that predict it. Therefore, the number of times t^* contributes to the weight update of $\mathbf{W}_{qk}$ as predicted token is on average smaller than the number of times it contributes as context token. It follows from Proposition S1.8 that the number of times the following is true,

$$\frac{\mathbb{E}\left[\|\Delta\mathbf{w}_{\cdot,k}\|^2\right]}{\mathbb{E}\left[\|\Delta\mathbf{w}_{m,\cdot}\|^2\right]} > 1, \tag{S97}$$

25

is on average higher than the number of times the following is true,

$$\frac{\mathbb{E}\left[\|\Delta\mathbf{w}_{\cdot,k}\|^2\right]}{\mathbb{E}\left[\|\Delta\mathbf{w}_{m,\cdot}\|^2\right]} < 1 \,. \tag{S98}$$

Therefore, the net increase of the norm of the columns is bigger than the net increase of the norm of the rows. We now prove that the number of columns with a high norm exceeds the number of rows with a high norm. At initialization, let each (k, m) entry of $\mathbf{W}_{qk}$ be an i.i.d. random variable drawn from a probability distribution with mean μ and variance σ^2. It follows that the mean norm of rows and columns are equal at initialization, as follows,

$$\mathbb{E}\left[|\mathbf{w}_{m,\cdot}|\right]\Big|_{\text{init}} = \mathbb{E}\left[|\mathbf{w}_{\cdot,k}|\right]\Big|_{\text{init}} = \mu \;\; \forall k, m \,. \tag{S99}$$

Furthermore, the variance of the norms of the rows σ^2_{rows} and of the columns σ^2_{cols} are equal at initialization,

$$\text{Var}\left(|\mathbf{w}_{m,\cdot}|\right)\Big|_{\text{init}} = \text{Var}\left(|\mathbf{w}_{\cdot,k,\cdot}|\right)\Big|_{\text{init}} = \sigma^2 \;\; \forall k, m \,. \tag{S100}$$

Therefore, the following inequality holds at the end of training,

$$\text{Var}\left(|\mathbf{w}_{m,\cdot}|\right) > \text{Var}\left(|\mathbf{w}_{\cdot,k}|\right) \;\; \forall k, m \,. \tag{S101}$$

Finally, we obtain from Lemma S1.11 that the following inequality holds,

$$\Pr[\|\mathbf{w}_{\cdot,k}\| > w] > \Pr[\|\mathbf{w}_{m,\cdot}\| > w] \;\; \forall w > \gamma \tag{S102}$$

where $\gamma = \sqrt{\text{Var}\left(|\mathbf{w}_{m,\cdot}|\right)\text{Var}\left(|\mathbf{w}_{\cdot,k}|\right)} - \mu$, thus concluding the proof. □

S1.4.5   Theorem on the emergence of symmetry

Finally, we prove that the weight updates of $\mathbf{W}_{qk}$ induce symmetry during bidirectional training. Importantly, the column dominance is present only during autoregressive training. Indeed, it follows from Proposition S1.10 that, during bidirectional training, the net increase of the norm of the columns is equal to the net increase of the norm of the rows. We formalize this in the following Corollary.

Corollary S1.13. *(Bidirectional training induces rows and columns with equal norm) Let $\mathcal{V} = [t_0, \dots, t_V]$ be a set of tokens. Let U be an ordered sequence of N tokens $U = [t_1, \dots, t_N]$ where $\Pr[t_j = t^*]$ is the probability that the token at index j in U is given by $t^* \in \mathcal{V}$. Let $\{\mathbf{x}_1 \dots, \mathbf{x}_n\}$ be the random embedding of the tokens as in Theorem S1.12. Let $\Delta\mathbf{W}_{qk}$ be the weight update of $\mathbf{W}_{qk}$ from Proposition 2.2. Let $\Delta\mathbf{W}_{qk}$ be derived from a bidirectional objective function as in Definition S1.3. Then, the variance of the norm of the rows and the columns at the end of training is equal,*

$$Var\left(|\mathbf{w}_{m,\cdot}|\right) = Var\left(|\mathbf{w}_{\cdot,k}|\right) \;\; \forall k, m \,. \tag{S103}$$

Proof. It follows from Proposition S1.10 that the number of times the following is true,

$$\frac{\mathbb{E}\left[\|\Delta\mathbf{w}_{\cdot,k}\|^2\right]}{\mathbb{E}\left[\|\Delta\mathbf{w}_{m,\cdot}\|^2\right]} > 1 \,, \tag{S104}$$

is on average equal to the number of times the following is true,

$$\frac{\mathbb{E}\left[\|\Delta\mathbf{w}_{\cdot,k}\|^2\right]}{\mathbb{E}\left[\|\Delta\mathbf{w}_{m,\cdot}\|^2\right]} < 1 \,. \tag{S105}$$

Therefore, the net increase of the norm of the columns is equal to the net increase of the norm of the rows. Following the same initialization assumptions as in Theorem S1.12, it follows that at the end of training,

$$\text{Var}\left(|\mathbf{w}_{m,\cdot}|\right) = \text{Var}\left(|\mathbf{w}_{\cdot,k}|\right) \;\; \forall k, m \,. \tag{S106}$$

thus concluding the proof. □

Now, we show that the bidirectional nature of the training objective is such that every pair of tokens (i, j) in a given sequence contributes to a term that is approximately symmetric. Here, we assume that predicting the i-th token from the j-th token is correlated to predicting the j-th token from the i-th token. In other words, predicting one token from the other gives similar predictions, that is, the term β_{ij} and β_{ji} from Proposition 2.2 are correlated. We formalize this in the following Theorem.

Theorem S1.14. *(**Bidirectional training induces symmetry**) Let U be an ordered sequence of N tokens $U = [t_1, \ldots, t_N]$. Let $\Delta \mathbf{W}_{qk}$ be derived from a bidirectional objective function as in Definition S1.3. It follows that the weight update of $\mathbf{W}_{qk}^l$ is given by*

$$\Delta \mathbf{W}_{qk}^l = \sum_{i=1}^{N} \sum_{j=1}^{N} \beta_{ij}^l \mathbf{K}_{ij}^{l-1}, \tag{S107}$$

and that every pair (i, j) with $i \neq j$ contributes to the weight update with a term

$$\Delta \mathbf{W}_{qk}^l \big|_{\mathbf{t}_i \leftrightarrow \mathbf{t}_j} = \beta_{ij}^l \mathbf{K}_{ij}^{l-1} + \beta_{ji}^l \mathbf{K}_{ij}^{l-1^T}, \tag{S108}$$

that is approximately symmetric,

$$\Delta \mathbf{W}_{qk}^l \big|_{\mathbf{t}_i \leftrightarrow \mathbf{t}_j} \approx \Delta \mathbf{W}_{qk}^l \big|_{\mathbf{t}_i \leftrightarrow \mathbf{t}_j}^\top. \tag{S109}$$

Proof. Let U be an ordered sequence of N tokens $U = [t_1, \ldots, t_N]$. It follows from Proposition 2.2 that the weight update for $\mathbf{W}_{qk}^l$ following the gradient of $\mathcal{L}(\mathbf{U})$ w.r.t. $\mathbf{W}_{qk}^l$ is given by

$$\Delta \mathbf{W}_{qk}^l = \sum_{i=1}^{N} \sum_{j=1}^{N} \beta_{ij}^l \mathbf{K}_{ij}^{l-1}, \tag{S110}$$

where we neglect any constant of proportionality - such as a learning rate - for simplicity. The double summation in Equation (S110) contains N^2 elements. We can rewrite the double summation as follows,

$$\sum_{i=1}^{N} \sum_{j=1}^{N} \beta_{ij}^l \mathbf{K}_{ij}^{l-1} = \sum_{i=1}^{N} \beta_{ii}^l \mathbf{K}_{ii}^{l-1} + \sum_{\substack{i,j=1 \\ i<j}}^{N} (\beta_{ij}^l \mathbf{K}_{ij}^{l-1} + \beta_{ji}^l \mathbf{K}_{ji}^{l-1}) \tag{S111}$$

where the first term includes the diagonal terms, and the second includes the contributions of every pair (i, j) with $i, j \in [0, \ldots, N]$. The second term can be written as,

$$\sum_{\substack{i,j=1 \\ i<j}}^{N} (\beta_{ij}^l \mathbf{K}_{ij}^{l-1} + \beta_{ji}^l \mathbf{K}_{ji}^{l-1}) = \sum_{\substack{i,j=1 \\ i<j}}^{N} (\beta_{ij}^l \mathbf{K}_{ij}^{l-1} + \beta_{ji}^l \mathbf{K}_{ij}^{l-1^\top}), \tag{S112}$$

and by decomposing $\mathbf{K}_{ij}^{l-1}$ in its symmetric and skew-symmetric parts, such that $\mathbf{K}_{ij}^{l-1} = \mathbf{S}_{ij}^{l-1} + \mathbf{N}_{ij}^{l-1}$, we obtain,

$$\sum_{\substack{i,j=1 \\ i<j}}^{N} (\beta_{ij}^l \mathbf{K}_{ij}^{l-1} + \beta_{ji}^l \mathbf{K}_{ij}^{l-1^\top}) = \sum_{\substack{i,j=1 \\ i<j}}^{N} [\beta_{ij}^l (\mathbf{S}_{ij}^{l-1} + \mathbf{N}_{ij}^{l-1}) + \beta_{ji}^l (\mathbf{S}_{ij}^{l-1} + \mathbf{N}_{ij}^{l-1})^T]$$

$$= \sum_{\substack{i,j=1 \\ i<j}}^{N} [(\beta_{ij}^l + \beta_{ji}^l) \mathbf{S}_{ij}^{l-1} + (\beta_{ij}^l - \beta_{ji}^l) \mathbf{N}_{ij}^{l-1}]. \tag{S113}$$

Let $\Delta \mathbf{W}_{qk}^l \big|_{\mathbf{t}_i \leftrightarrow \mathbf{t}_j} = \beta_{ij}^l \mathbf{K}_{ij}^{l-1} + \beta_{ji}^l \mathbf{K}_{ij}^{l-1^T}$, and let β_{ij}^l and β_{ji}^l be such that $\text{sign}(\beta_{ij}^l) = \text{sign}(\beta_{ji}^l)$ and $|\beta_{ij}^l| \approx |\beta_{ji}^l|$. It follows that

$$\Delta \mathbf{W}_{qk}^l \big|_{\mathbf{t}_i \leftrightarrow \mathbf{t}_j} \approx \sum_{\substack{i,j=1 \\ i<j}}^{N} \beta_{ij}^l \mathbf{S}_{ij}^{l-1} = \sum_{\substack{i,j=1 \\ i<j}}^{N} \beta_{ij}^l \mathbf{S}^{l-1^\top}_{ij} = \Delta \mathbf{W}_{qk}^l {}^\top \big|_{\mathbf{t}_i \leftrightarrow \mathbf{t}_j} \tag{S114}$$

thus concluding the proof. □

Encoder-only models are typically not trained to predict every token in a sequence, but rather a random subset of tokens, and the model can attend to tokens bidirectionally. This is usually called Masked Language Modeling (MLM) [Devlin et al., 2019, Liu et al., 2019, Lan et al., 2020, Warner et al., 2024]. Therefore, only a subset of terms in the double summation of Equation (S113) has the symmetric properties described above. We generalize the proof to this case in the following.

Remark S1.15. Let $C_i = [0, 1, \ldots, N]$ and let the summation indexed by i to run over a random subset of tokens $M \subset [0, 1, \ldots, N]$. The weight update of $\mathbf{W}_{qk}$ is then given by

$$\Delta \mathbf{W}_{qk}^l = \sum_{i \in M} \sum_{j=1}^{N} \beta_{ij}^l \mathbf{K}_{ij}^{l-1} \,. \tag{S115}$$

The double summation contains $N|M|$ elements, where $|M|$ is the cardinality of the subset M. We can rewrite the double summation as follows,

$$\sum_{i \in M} \sum_{j=1}^{N} \beta_{ij}^l \mathbf{K}_{ij}^{l-1} = \sum_{i \in M} \beta_{ii}^l \mathbf{K}_{ii}^{l-1} + \sum_{\substack{i,j \in M \\ i<j}} (\beta_{ij}^l \mathbf{K}_{ij}^{l-1} + \beta_{ji}^l \mathbf{K}_{ji}^{l-1}) + \sum_{i \in M} \sum_{j \in \bar{M}} \beta_{ij}^l \mathbf{K}_{ij}^{l-1}, \tag{S116}$$

where the first term includes the diagonal terms, the second includes the contributions of the pairs (i, j) with $i, j \in M$, and the third includes the remaining terms with $\bar{M} = [1, \ldots, N] \setminus M$. The second term can be written as,

$$\sum_{\substack{i,j \in M \\ i<j}} (\beta_{ij}^l \mathbf{K}_{ij}^{l-1} + \beta_{ji}^l \mathbf{K}_{ji}^{l-1}) = \sum_{\substack{i,j \in M \\ i<j}} (\beta_{ij}^l \mathbf{K}_{ij}^{l-1} + \beta_{ji}^l \mathbf{K}_{ij}^{l-1^\top}), \tag{S117}$$

and by decomposing $\mathbf{K}_{ij}^{l-1}$ in its symmetric and skew-symmetric parts, such that $\mathbf{K}_{ij}^{l-1} = \mathbf{S}_{ij}^{l-1} + \mathbf{N}_{ij}^{l-1}$, we obtain,

$$
\begin{aligned}
\sum_{\substack{i,j \in M \\ i<j}} (\beta_{ij}^l \mathbf{K}_{ij}^{l-1} + \beta_{ji}^l \mathbf{K}_{ij}^{l-1^\top}) &= \sum_{\substack{i,j \in M \\ i<j}} [\beta_{ij}^l (\mathbf{S}_{ij}^{l-1} + \mathbf{N}_{ij}^{l-1}) + \beta_{ji}^l (\mathbf{S}_{ij}^{l-1} + \mathbf{N}_{ij}^{l-1})^T] \\
&= \sum_{\substack{i,j \in M \\ i<j}} [(\beta_{ij}^l + \beta_{ji}^l) \mathbf{S}_{ij}^{l-1} + (\beta_{ij}^l - \beta_{ji}^l) \mathbf{N}_{ij}^{l-1}],
\end{aligned}
\tag{S118}
$$

with a similar structure as in Equation (S113).

Let $|M| = pN$ with $0 < p < 1$ being the percentage of tokens to be predicted during bidirectional training. The total number of pairs in the second term of Equation (S116) is given by a binomial coefficient, thus the total number of elements in the summation is $pN(pN - 1)$. The total number of elements in the third term is instead the product $pN(N - pN)$. Therefore, the percentage of symmetric weight updates from the second term over the total number of updates in the third term is given by

$$\frac{pN(pN - 1)}{pN(N - pN)} \approx \frac{pN}{(N - pN)}, \tag{S119}$$

in the limit of large N. In practice, p is set to be around 15%-30% [Devlin et al., 2019, Liu et al., 2019, Lan et al., 2020, Warner et al., 2024], leading to $\approx 25\%$ of symmetric weight updates on average.

S1.5. Properties of the symmetry score in Definition 3.1 and related proofs

The score s we introduce in Section 3 indicates the *degree* of symmetry of a matrix $\mathbf{M}$ by quantifying the contribution to the Frobenious norm of its symmetric and skew-symmetric parts. In particular, s equals 1 and -1 for a fully symmetric and skew-symmetric matrix. Accordingly, positive (negative) values of s indicate the presence of symmetric (skew-symmetric) structures. Here, we provide a proof for these properties. First, we show that the Frobenious norm of any square matrix $\mathbf{M}$ can be decomposed in the sum of the Frobenious norm of its symmetric and skew-symmetric components, as in the following Lemma,

Lemma S1.16. *For any square matrix $\mathbf{M} \in \mathbb{M}_n$ the following equivalence holds*

$$\|\mathbf{M}\|_F^2 = \|\mathbf{M}_s\|_F^2 + \|\mathbf{M}_n\|_F^2 . \tag{S120}$$

Proof. The Frobenius norm of a matrix $\mathbf{M}$ can be defined as $\|\mathbf{M}\|_F = \sqrt{\mathrm{Tr}(\mathbf{MM}^\top)}$, and as such we observe that for any square matrix $\mathbf{M}$ we get

$$\begin{aligned}
\|\mathbf{M}\|_F &= \sqrt{\mathrm{Tr}(\mathbf{MM}^\top)} = \sqrt{\mathrm{Tr}((\mathbf{M}_s + \mathbf{M}_n)(\mathbf{M}_s + \mathbf{M}_n)^\top)} = \\
&= \sqrt{\mathrm{Tr}(\mathbf{M}_s\mathbf{M}_s^\top) + \mathrm{Tr}(\mathbf{M}_s\mathbf{M}_n^\top) + \mathrm{Tr}(\mathbf{M}_n\mathbf{M}_s^\top) + \mathrm{Tr}(\mathbf{M}_n\mathbf{M}_n^\top)} .
\end{aligned} \tag{S121}$$

It follows from the cyclic property of the trace operator that the mixing terms cancel out as follows,

$$\mathrm{Tr}(\mathbf{M}_s\mathbf{M}_n^\top) + \mathrm{Tr}(\mathbf{M}_n\mathbf{M}_s^\top) = -\mathrm{Tr}(\mathbf{M}_s\mathbf{M}_n) + \mathrm{Tr}(\mathbf{M}_s\mathbf{M}_n) = 0 , \tag{S122}$$

resulting in

$$\|\mathbf{M}\|_F = \sqrt{\mathrm{Tr}(\mathbf{M}_s\mathbf{M}_s^\top) + \mathrm{Tr}(\mathbf{M}_n\mathbf{M}_n^\top)} . \tag{S123}$$

Therefore, as both terms on the right-hand side are semi-positive definite, we conclude the proof as follows,

$$\|\mathbf{M}\|_F^2 = \mathrm{Tr}(\mathbf{M}_s\mathbf{M}_s^\top) + \mathrm{Tr}(\mathbf{M}_n\mathbf{M}_n^\top) = \|\mathbf{M}_s\|_F^2 + \|\mathbf{M}_n\|_F^2 . \tag{S124}$$

$\square$

Next, we formulate the properties of the symmetry score as follows,

Proposition S1.17. *The symmetry score s quantifies the degree of symmetry or skew-symmetry of a given square matrix $\mathbf{M}$. In particular,*
1) The symmetry score s is a scalar value bounded in the range $[-1, 1]$.
2) A symmetry score $s = \pm 1$ indicates a fully symmetric or skew-symmetric matrix, respectively.
3) The symmetry score of a random matrix $\mathbf{M} \in \mathbb{M}_n$ with entries $\mathbf{M}_{ij} \sim p(0, \sigma)$ from a probability distribution with zero mean and finite variance tends to zero as $8/n$ in the limit $n \to \infty$.

Proof. To prove the points (1) and (2), we first show that it follows from Lemma S1.16 that the squared Frobenious norm of $\mathbf{M}_s$ and $\mathbf{M}_n$ are in an orthogonal relation

$$\|\mathbf{M}\|_F = \sqrt{\|\mathbf{M}_s\|_F^2 + \|\mathbf{M}_n\|_F^2} . \tag{S125}$$

Therefore, for any given $\mathbf{M}$, the norms $\|\mathbf{M}_s\|_2^2$ and $\|\mathbf{M}_n\|_2^2$ are such that a higher value of the first leads to to a lower value of the second, and vice versa. In particular, it is straightforward to observe that $\|\mathbf{M}_s\|_2 = \|\mathbf{M}\|_2$ and $\|\mathbf{M}_n\|_2 = 0$ if $\mathbf{M}$ is symmetric. Next, we derive a decomposition of the squared Frobenious norm of the symmetric and skew-symmetric part of $\mathbf{M}$. From the definition of $\mathbf{M}_s$ we obtain that

$$\begin{aligned}
\|\mathbf{M}_s\|_F^2 &= \mathrm{Tr}(\mathbf{M}_s\mathbf{M}_s^\top) = \frac{1}{4}\,\mathrm{Tr}[(\mathbf{M} + \mathbf{M}^\top)(\mathbf{M}^\top + \mathbf{M})] \\
&= \frac{1}{4}\left[\mathrm{Tr}(\mathbf{MM}^\top) + \mathrm{Tr}(\mathbf{MM}) + \mathrm{Tr}(\mathbf{M}^\top\mathbf{M}^\top) + \mathrm{Tr}(\mathbf{M}^\top\mathbf{M})\right] \\
&= \frac{1}{2}\left[\mathrm{Tr}(\mathbf{MM}^\top) + \mathrm{Tr}(\mathbf{MM})\right] \\
&= \frac{1}{2}\left[\|\mathbf{M}\|_F^2 + \mathrm{Tr}(\mathbf{MM})\right] .
\end{aligned} \tag{S126}$$

Since the upper bound for $\|\mathbf{M}_s\|_F^2$ is given by $\|\mathbf{M}\|_F^2$, the second term on the left-hand side has an upper bound given by,

$$\mathrm{Tr}(\mathbf{MM}) \leq \frac{1}{2}\|\mathbf{M}\|_F^2 , \tag{S127}$$

29

A complementary relation holds for the skew-symmetric component of $\mathbf{M}$,

$$\|\mathbf{M_n}\|_F^2 = \frac{1}{4} \text{Tr}[(\mathbf{M} - \mathbf{M}^\top)(\mathbf{M}^\top - \mathbf{M})] = \frac{1}{2} \left[\|\mathbf{M}\|_F^2 - \text{Tr}(\mathbf{MM})\right], \tag{S128}$$

which, following the same logic, defines a lower-bound for $\text{Tr}(\mathbf{MM})$ as follows,

$$-\frac{1}{2}\|\mathbf{M}\|_F^2 \leq \text{Tr}(\mathbf{MM}). \tag{S129}$$

Given Definition 3.1 we can write,

$$s = \frac{\|\mathbf{M}\|_F^2 + \text{Tr}(\mathbf{MM}) - \|\mathbf{M}\|_F^2 + \text{Tr}(\mathbf{MM})}{\|\mathbf{M}\|_F^2} = 2\frac{\text{Tr}(\mathbf{MM})}{\|\mathbf{M}\|_F^2} \tag{S130}$$

and by combining the bounds derived previously we obtain,

$$-1 \leq s \leq 1 \tag{S131}$$

with

$$\begin{cases} s = 1 & \text{if} \quad \mathbf{M} = \mathbf{M}^\top \\ s = -1 & \text{if} \quad \mathbf{M} = -\mathbf{M}^\top \end{cases} \tag{S132}$$

To prove the point (3), let each entry $m_{ij} = [\mathbf{M}]_{ij}$ be an independent, identically distributed sample from a random distribution with mean zero and a finite variance σ^2. We compute the Frobenius norm of the symmetric and skew-symmetric parts as follows,

$$\|\mathbf{M}_s\|_F^2 = \sum_{i \neq j} \left(\mathbf{M}_{ij} + \mathbf{M}_{ji}\right)^2 + \sum_i (2\mathbf{M}_{ii})^2$$

$$\|\mathbf{M}_n\|_F^2 = \sum_{i \neq j} \left(\mathbf{M}_{ij} - \mathbf{M}_{ji}\right)^2. \tag{S133}$$

Here, the skew-symmetric part has a zero diagonal term (because of the subtraction), and the symmetric part has twice the diagonal of the original matrix $\mathbf{M}$ (because of the addition). Since the entries are independent, $\mathbf{M}_{ij}$ is independent of $\mathbf{M}_{ji}$ for all $j \neq i$, and thus we can treat the off-diagonal entries of the $\mathbf{M}_s$ and $\mathbf{M}_n$ terms as a sum and difference of two independent random samples having mean zero and the same variance. It follows that the resulting distribution has a mean zero and a variance of $2\sigma^2$ in both cases,

$$\sum_{i \neq j} \left(\mathbf{M}_{ij} \pm \mathbf{M}_{ji}\right)^2 = 2 \sum_{i=1}^n \sum_{j=i+1}^n \left(\mathbf{M}_{ij} \pm \mathbf{M}_{ji}\right)^2 \underset{n \to \infty}{\approx} n(n-1)\text{Var}\left[\mathbf{M}_{ij} \pm \mathbf{M}_{ji}\right] = n(n-1)2\sigma^2, \tag{S134}$$

where the approximation is due to the central limit theorem. Applying a similar logic to the second term on the symmetric norm, each entry is the double of a random i.i.d. distribution with

$$\sum_{i=1}^N (2\mathbf{M}_{ii})^2 \underset{N \to \infty}{\approx} n\text{Var}\left[\mathbf{M}_{ij}\right] = n4\sigma^2. \tag{S135}$$

Finally, we take the Frobenius norm of the random matrix itself and apply the same logic, where there are n^2 entries with a variance of σ^2,

$$\|\mathbf{M}\|_F^2 \underset{n \to \infty}{\approx} n^2\sigma^2. \tag{S136}$$

It follows that the symmetry score is given by

$$s = 2\frac{\|\mathbf{M}_s\|_F^2 - \|\mathbf{M}_n\|_F^2}{\|\mathbf{M}\|_F^2} \underset{n \to \infty}{\approx} \frac{8\sigma^2 n}{\sigma^2 n^2} = \frac{8}{n}, \tag{S137}$$

where the symmetry score is zero in the limit $n \to \infty$ with convergence from the positive side. $\qquad\square$

S1.6. Properties of the directionality score in Definition 3.2 and related proofs

The score d we introduce in Section 3 quantifies the directional bias of a square matrix $\mathbf{M}$ by comparing the total norm of the "outliers" rows and columns, that is, that are higher than γ times the standard deviations of the norms. A directionality score d of 1 indicates the presence of rows with high "outlier" norms and the absence of outliers in the distribution of the column norms. The opposite is true for a directionality score d of -1. Accordingly, positive (negative) values of d indicate the presence of row (column) dominance in the matrix. Here, we provide a proof for these properties.

Proposition S1.18. *The symmetry score d provides a quantitative measure of the degree of directional bias in a given square matrix $\mathbf{M}$.*
1) The directionality score d is a scalar value that lies within the range $[-1, 1]$.
2) For any given $\gamma > 0$, a directionality score $d = \pm 1$ indicates that vectors satisfying the condition defined by γ are exclusively present in the rows or the column distribution, respectively.
3) The directionality score of a random matrix $\mathbf{M} \in \mathbb{M}_n$ with entries $\mathbf{M}_{ij} \sim p(0, \sigma)$ from a probability distribution with zero mean and a variance that scales as $O(n^{-1})$ tends to zero in the limit $n \to \infty$.

Proof. To prove that the directionality score is bounded in the interval $[-1, 1]$, note that $\bar{c}_{\mathbf{M}}, \bar{r}_{\mathbf{M}} > 0$ simply because they are sums of norms. As both are positive,

$$|\bar{c}_{\mathbf{M}} - \bar{r}_{\mathbf{M}}| < \bar{c}_{\mathbf{M}} < \bar{c}_{\mathbf{M}} + \bar{r}_{\mathbf{M}} \tag{S138}$$

and thus

$$\frac{\bar{c}_{\mathbf{M}} - \bar{r}_{\mathbf{M}}}{\bar{c}_{\mathbf{M}} + \bar{r}_{\mathbf{M}}} < 1 \tag{S139}$$

and taking the negative sign for the absolute value,

$$-\frac{\bar{r}_{\mathbf{M}} - \bar{c}_{\mathbf{M}}}{\bar{c}_{\mathbf{M}} + \bar{r}_{\mathbf{M}}} > -1 \Rightarrow \frac{\bar{c}_{\mathbf{M}} - \bar{r}_{\mathbf{M}}}{\bar{c}_{\mathbf{M}} + \bar{r}_{\mathbf{M}}} > -1. \tag{S140}$$

In the extremes $d = \pm 1$, the numerator must be equal to the denominator in absolute value, implying that either $\bar{r}_{\mathbf{M}}$ or $\bar{c}_{\mathbf{M}}$ are zero and the other is positive. For completeness, we define the score as zero if both are zero.

Finally, we study the case of a random matrix. We start by noting that the values of $\bar{r}_{\mathbf{M}}$, $\bar{c}_{\mathbf{M}}$ are interchanged when we take the transpose, hence

$$\bar{r}_{\mathbf{M}} = \bar{c}_{\mathbf{M}^\top} \tag{S141}$$

Regardless of the scaling of the matrix and the value γ, the key property of a random matrix is that all entries are drawn from the same distribution. Hence,

$$\Pr\left[\mathbf{M}_{ij} = x\right] = \Pr\left[\mathbf{M}_{ji} = x\right] \Rightarrow \Pr[\mathbf{M} = \mathbf{X}] = \Pr\left[\mathbf{M} = \mathbf{X}^\top\right] \tag{S142}$$

for x and $\mathbf{X}$ being any arbitrary value or matrix. As a consequence,

$$\Pr[\bar{c}_{\mathbf{M}} = x] = \Pr[\bar{c}_{\mathbf{M}^\top} = x] = \Pr[\bar{r}_{\mathbf{M}} = x] \tag{S143}$$

where the last equality comes from Eq. S141. The main point here is that the probability distribution of both rows and columns is the same. Pushing this forward, the expected value of $\bar{r}_{\mathbf{M}} - \bar{c}_{\mathbf{M}}$ is

$$\mathrm{E}\left[\bar{r}_{\mathbf{M}} - \bar{c}_{\mathbf{M}}\right] = \mathrm{E}\left[\bar{r}_{\mathbf{M}}\right] - \mathrm{E}\left[\bar{c}_{\mathbf{M}}\right] = \int \bar{c}_{\mathbf{M}} \Pr[\mathbf{M}] \, d\mathbf{M} - \int \bar{r}_{\mathbf{M}} \Pr[\mathbf{M}] \, d\mathbf{M} \tag{S144}$$

$$= \int \bar{r}_{\mathbf{M}} \Pr\left[\mathbf{M}^\top\right] d\mathbf{M}^\top - \int \bar{r}_{\mathbf{M}} \Pr[\mathbf{M}] \, d\mathbf{M} = 0 \tag{S145}$$

Furthermore, the expected value of $\bar{r}_{\mathbf{M}} + \bar{c}_{\mathbf{M}}$ is strictly positive, since both values are positive. Thus, their ratio, the directionality score of a random matrix, is zero.

Configuration	BERT	BERT-Mini
Hidden Size	768	256
Intermediate Size	3072	1024
Number of Attention Heads	12	4
Number of Hidden Layers	12	4
Attention Dropout Probability	0.1	0.1
Hidden Activation Function	gelu	gelu
Hidden Dropout Probability	0.1	0.1
Layer Normalization Epsilon	1e-12	1e-12
Max Position Embeddings	512	512
Position Embedding Type	absolute	absolute
Vocabulary Size	30522	30522

Table S1: Configurations for BERT and BERT-Mini models.

Notice that to be thorough we must show that their variance is bounded scales down. Since weight initialization has been extensively studied, we will just make a general reference to it here. In machine learning, all weights are initialized with zero mean and variances that scale as $O(n^{-1})$. As $\mathbf{M}$ is a product of two matrices with such scaling, each entry would consist of the sum of n random variables, where each one has a scaling of $O(n^{-2})$ since it is the product of two random variables with an $O(n^{-1})$ scaling. Thus, the entries of $\mathbf{M}$ also have a scaling of $O(n^{-1})$. Applying the mean value theorem gives us the desired result.

$\square$

S2. Experimental Details

We trained two BERT models [Devlin et al., 2019] to examine the evolution of the symmetry and directionality scores throughout the training process. Detailed information regarding the training procedure is provided below.

S2.1. Models

We train the standard BERT model (referred to as *BERT*) and a smaller version (referred to as *BERT-Mini*), following the implementation by [Devlin et al., 2019]. Table S1 provides an overview of the model parameters. The standard BERT model has 12 layers, 12 attention heads, and embedding dimensions of 768 for the hidden layers and 3072 for the intermediate layers. In contrast, the smaller BERT-Mini model uses 4 layers, 4 attention heads, and embedding dimensions of 256 and 1024, respectively.

Initialization We optionally initialize the models with either symmetric or skew-symmetric attention weights by initializing the key and query weight matrices of all self-attention blocks following a specific procedure. For symmetric initialization, the query weight matrix $\mathbf{W_q}$ is initialized randomly, and then the key weight matrix is set to $\mathbf{W_k} = \mathbf{W_q}$. For skew-symmetric initialization, $\mathbf{W_q}$ is initialized randomly, and a skew-symmetric matrix $\mathbf{S}$ is generated by first initializing a random matrix, $\mathbf{A}$ and then calculating $\mathbf{S} = \mathbf{A} - \mathbf{A}^\top$. The key matrix is then defined as $\mathbf{W_k} = \mathbf{W_q}\mathbf{S}^\top$, ensuring that the matrix multiplication $\mathbf{W_q}\mathbf{W_k}^\top$ is skew-symmetric.

Loss Constraints The loss function $\mathcal{L}(\mathbf{U})$ described in Equation (S22) is optionally extended with a constraint to either encourage symmetric or skew-symmetric attention weights.

$$\mathcal{L}(\mathbf{U}) := \mathcal{L}(\mathbf{U}) + \gamma\mathcal{L}_c(\mathcal{W}). \tag{S146}$$

32

Here, γ is a coefficient defining the importance of the $\mathcal{L}_c$ constraint. To encourage symmetry, we minimize the condition

$$\mathcal{L}_c(\mathcal{W}) = \frac{\mathbf{M}^2}{\mathbf{M}_s^2}. \tag{S147}$$

This constraint reaches its minimum if all attention weights have a symmetry score $s = 1$. To encourage skew-symmetry, we minimize the condition

$$\mathcal{L}_c(\mathcal{W}) = \frac{\mathbf{M}^2}{\mathbf{M}_n^2}, \tag{S148}$$

leading to a symmetry score of $s = 0$.

S2.2. Datasets

The models are trained on three datasets. First, we use the "20220301.en" snapshot from the Wikipedia dataset, which consists of 6.46 million samples crawled from Wikipedia. Second, we utilize the Jigsaw dataset with 159K samples, originally collected for a toxic comment classification challenge. Finally, we train on the English "2023-14" snapshot of the RedPajama-V2 dataset, which contains approximately 5.12 billion samples.

S2.3. Training Settings

The models are trained for $200,000$ update steps with a batch size of 32 and 8 gradient accumulation steps, effectively increasing the batch size to 256 before each parameter update. The optimization is done using the AdamW optimizer [Loshchilov and Hutter, 2019], and the training schedule includes 200 warmup steps to stabilize early training, followed by a linear decay learning rate schedule, starting at an initial learning rate of 5×10^{-5} and weight decay of 0.01. Mixed precision (fp16) training was utilized to maximize training efficiency, which reduces memory consumption and speeds up computation without significant loss of precision. The training data was processed with a masked language modeling (MLM) probability of 15%, ensuring that 15% of tokens were masked during training. The models are trained in the encoder and decoder mode, i.e., to predict masked tokens and subsequent tokens respectively.
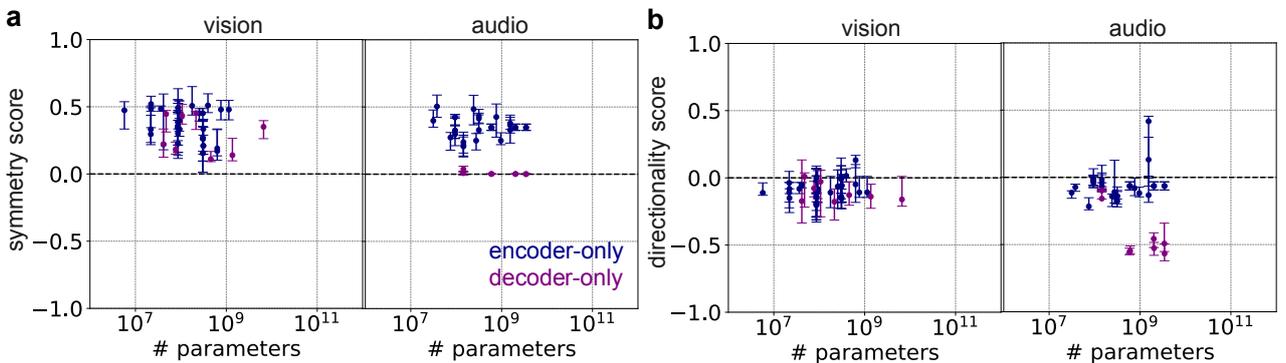
S3. Supplementary Figures

Figure S1: **a)** Median symmetry score of the matrix $\mathbf{W}_{qk}$ as a function of the total number of parameters for vision and audio models. Each dot corresponds to the median and the interquartile range across layers of a given pre-trained model. **b)** Same as in **a** for the median directionality score of the matrix $\mathbf{W}_{qk}$.
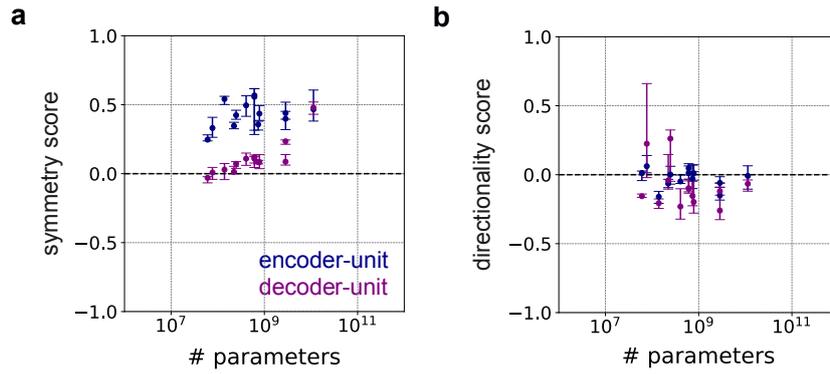
Figure S2: **a**) Median symmetry score of the matrix $\mathbf{W}_{qk}$ as a function of the total number of parameters for vision and audio models. Each dot corresponds to the median and the interquartile range across layers of the encoder component (blue) and decoder component (purple) of an encoder-decoder Transformer model. The encoder component of these models shows a high degree of symmetry compared to the decoder component. **b**) Same as in **a** for the median directionality score of the matrix $\mathbf{W}_{qk}$. The encoder and decoder components of these models do not show significant differences in directionality scores.

S4. Supplementary Tables

Table S2: Symmetry score for open-source pretrained language models. All models are available on Hugging Face [Wolf et al., 2020].

Model	Median	Interquartile range	Model	Median	Interquartile range
BERT-tiny	0.77	± [0.07, 0.07]	GPT-Neo1.3B	0.14	± [0.03, 0.03]
BERT-mini	0.62	± [0.03, 0.05]	GPT-Neo2.7B	0.13	± [0.02, 0.04]
BERT-small	0.69	± [0.10, 0.08]	GPT-J6B	0.11	± [0.02, 0.03]
BERT-medium	0.60	± [0.01, 0.02]	OpenAI-GPT	0.07	± [0.04, 0.03]
BERT-base	0.51	± [0.09, 0.07]	GPT2-XL	0.12	± [0.03, 0.05]
BERT-large	0.44	± [0.03, 0.08]	DistilGPT2	0.19	± [0.05, 0.05]
DistilBERT	0.43	± [0.10, 0.13]	GPT-Neo125M	0.14	± [0.09, 0.14]
BERT-2L-128	0.77	± [0.07, 0.07]	GPT-Neo1.3B	0.14	± [0.03, 0.03]
BERT-4L-256	0.62	± [0.03, 0.05]	GPT-Neo2.7B	0.14	± [0.03, 0.02]
BERT-4L-512	0.69	± [0.10, 0.08]	GPT-J6B	0.11	± [0.02, 0.03]
BERT-8L-512	0.60	± [0.01, 0.02]	LLaMA2-7B	0.12	± [0.02, 0.03]
BERT-base	0.51	± [0.09, 0.07]	LLaMA2-13B	0.17	± [0.02, 0.02]
BERT-large	0.44	± [0.03, 0.08]	LLaMA3-8B	0.00	± [0.00, 0.01]
DistilBERT	0.43	± [0.10, 0.13]	LLaMA3.1-8B	0.00	± [0.00, 0.01]
BEiT-base	0.40	± [0.08, 0.02]	LLaMA3.2-8B	0.01	± [0.01, 0.01]
BEiT-large	0.33	± [0.05, 0.07]	LLaMA3.2-1B	0.01	± [0.01, 0.01]
BEiT-base	0.39	± [0.23, 0.07]	LLaMA3.2-3B	0.01	± [0.01, 0.01]
BEiT-large	0.26	± [0.17, 0.13]	LLaMA2-7B-chat	0.12	± [0.02, 0.03]
BEiT-base	0.39	± [0.23, 0.07]	LLaMA2-70B	0.02	± [0.01, 0.02]
BEiT-large	0.26	± [0.17, 0.13]	LLaMA2-7B-chat	0.12	± [0.02, 0.03]
BEiT-large	0.26	± [0.17, 0.13]	LLaMA2-13B-chat	0.17	± [0.02, 0.02]
ALBERT-base	0.72	± [0.00, 0.00]	LLaMA3-8B	0.00	± [0.00, 0.00]
ALBERT-large	0.70	± [0.00, 0.00]	LLaMA3-70B	0.02	± [0.01, 0.01]
ALBERT-xlarge	0.59	± [0.00, 0.00]	LLaMA3.1-8B	0.00	± [0.00, 0.01]
ALBERT-xxlarge	0.46	± [0.00, 0.00]	LLaMA3.1-70B	0.01	± [0.00, 0.01]
RoBERTa-base	0.49	± [0.03, 0.06]	LLaMA3.1-405B	0.03	± [0.01, 0.03]
RoBERTa-large	0.47	± [0.06, 0.06]	LLaMA3.2-1B	0.00	± [0.00, 0.00]
XLM-R-base	0.51	± [0.05, 0.03]	LLaMA3.2-3B	0.01	± [0.01, 0.01]
XLM-R-large	0.49	± [0.16, 0.12]	Mistral-7B	0.00	± [0.00, 0.01]
RoBERTa-mnli	0.47	± [0.06, 0.06]	Mixtral-8x22B	0.00	± [0.00, 0.00]
DistilRoBERTa	0.53	± [0.02, 0.06]	MobileLLM125M	0.03	± [0.02, 0.03]
ModernBERT-base	0.18	± [0.06, 0.18]	MobileLLM350M	0.01	± [0.01, 0.01]
GPT1	0.07	± [0.04, 0.03]	Phi-1.5	0.09	± [0.03, 0.03]
GPT2	0.15	± [0.02, 0.03]	Phi-1	0.14	± [0.02, 0.01]
GPT2-medium	0.17	± [0.03, 0.05]	Phi-2	0.07	± [0.03, 0.06]

Table S3: Directionality score for open-source pretrained language models. All models are available on Hugging Face [Wolf et al., 2020].

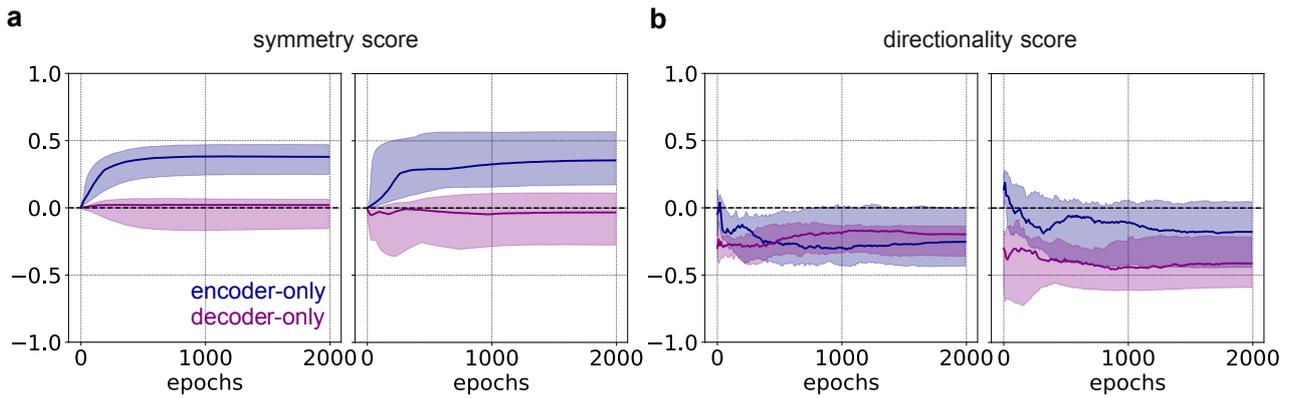| Model	Median	Interquartile range	Model	Median	Interquartile range
BERT-tiny	-0.79	± [0.11, 0.11]	GPT-Neo1.3B	-0.49	± [0.19, 0.13]
BERT-mini	-0.33	± [0.03, 0.04]	GPT-Neo2.7B	-0.57	± [0.15, 0.16]
BERT-small	-0.22	± [0.04, 0.03]	GPT-J6B	-0.28	± [0.09, 0.08]
BERT-medium	-0.23	± [0.06, 0.10]	OpenAI-GPT	-0.18	± [0.08, 0.07]
BERT-base	-0.08	± [0.02, 0.03]	GPT2-XL	-0.23	± [0.11, 0.10]
BERT-large	-0.03	± [0.02, 0.06]	DistilGPT2	-0.51	± [0.03, 0.07]
DistilBERT	-0.13	± [0.00, 0.06]	GPT-Neo125M	-0.56	± [0.21, 0.08]
BERT-2L-128	-0.79	± [0.11, 0.11]	GPT-Neo1.3B	-0.49	± [0.19, 0.13]
BERT-4L-256	-0.33	± [0.03, 0.04]	GPT-Neo2.7B	-0.49	± [0.15, 0.21]
BERT-4L-512	-0.22	± [0.04, 0.03]	GPT-J6B	-0.28	± [0.09, 0.08]
BERT-8L-512	-0.23	± [0.06, 0.10]	LLaMA2-7B	-0.26	± [0.09, 0.13]
BERT-base	-0.08	± [0.02, 0.03]	LLaMA2-13B	-0.15	± [0.11, 0.03]
BERT-large	-0.03	± [0.02, 0.06]	LLaMA3-8B	-0.65	± [0.13, 0.20]
DistilBERT	-0.13	± [0.00, 0.06]	LLaMA3.1-8B	-0.64	± [0.17, 0.19]
BEiT-base	-0.10	± [0.06, 0.15]	LLaMA3.2-8B	-0.59	± [0.18, 0.22]
BEiT-large	-0.15	± [0.08, 0.07]	LLaMA3.2-1B	-0.59	± [0.18, 0.22]
BEiT-base	-0.14	± [0.15, 0.21]	LLaMA3.2-3B	-0.77	± [0.08, 0.19]
BEiT-large	-0.14	± [0.04, 0.14]	LLaMA2-7B-chat	-0.29	± [0.07, 0.14]
BEiT-base	-0.14	± [0.15, 0.21]	LLaMA2-70B	-0.24	± [0.10, 0.06]
BEiT-large	-0.14	± [0.04, 0.14]	LLaMA2-7B-chat	-0.29	± [0.07, 0.14]
BEiT-large	-0.15	± [0.03, 0.14]	LLaMA2-13B-chat	-0.19	± [0.12, 0.04]
ALBERT-base	-0.07	± [0.00, 0.00]	LLaMA3-8B	0.01	± [0.05, 0.05]
ALBERT-large	-0.17	± [0.00, 0.00]	LLaMA3-70B	-0.37	± [0.09, 0.12]
ALBERT-xlarge	-0.24	± [0.00, 0.00]	LLaMA3.1-8B	-0.57	± [0.16, 0.13]
ALBERT-xxlarge	-0.15	± [0.00, 0.00]	LLaMA3.1-70B	-0.37	± [0.08, 0.11]
RoBERTa-base	-0.12	± [0.11, 0.03]	LLaMA3.1-405B	-0.17	± [0.07, 0.07]
RoBERTa-large	-0.06	± [0.03, 0.03]	LLaMA3.2-1B	-0.02	± [0.13, 0.08]
XLM-R-base	-0.02	± [0.02, 0.02]	LLaMA3.2-3B	-0.70	± [0.07, 0.22]
XLM-R-large	-0.02	± [0.03, 0.02]	Mistral-7B	-0.58	± [0.15, 0.13]
RoBERTa-mnli	-0.06	± [0.03, 0.03]	Mixtral-8x22B	-0.66	± [0.09, 0.16]
DistilRoBERTa	-0.14	± [0.09, 0.07]	MobileLLM125M	-0.13	± [0.15, 0.10]
ModernBERT-base	-0.04	± [0.05, 0.04]	MobileLLM350M	-0.34	± [0.13, 0.23]
GPT1	-0.18	± [0.08, 0.07]	Phi-1.5	-0.28	± [0.22, 0.19]
GPT2	-0.58	± [0.06, 0.14]	Phi-1	-0.40	± [0.03, 0.04]

Figure S3: **a**) Evolution of symmetry score during training. Shown are the median and the interquartile range. Models were trained on the Jigsaw dataset [cjadams et al., 2017] (left) and on the Red Pajama dataset [Computer, 2023] (right). Encoder-only and decoder-only models are color-coded in blue and purple, respectively (see legend). **b**) Same as in panel **a** for the median directionality score.
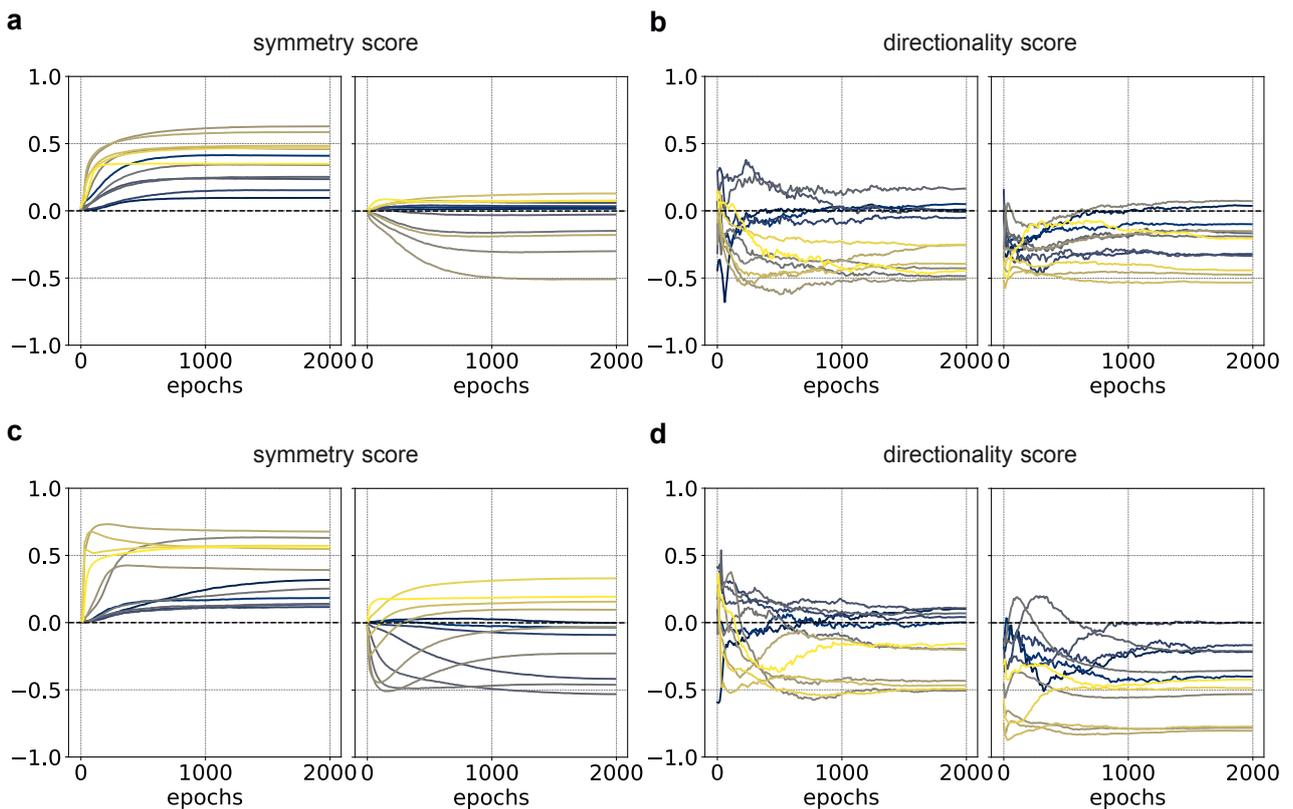

Figure S4: **a**) Evolution of the median symmetry score across layers of the encoder-only (left) and decoder-only (right) models. Each layer is color-coded as shown on the legend of Figure 3. Shown are the median and the interquartile range. Models were trained on the Jigsaw dataset [cjadams et al., 2017]. **b**) Same as in panel **a** for the median directionality score. **c**) Same as in panel **a** for models trained on the Red Pajama dataset [Computer, 2023]. **d**) Same as panel **c** for the median directionality score.
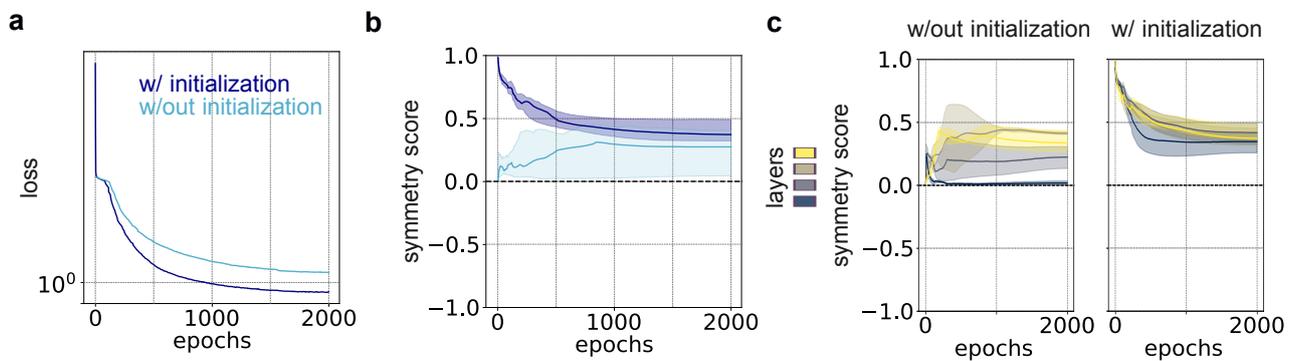
Figure S5: **a**) Loss a 4-layer encoder-only model with (dark blue) and without (light blue) symmetric initialization, respectively. Models are trained on the Red Pajama dataset [Computer, 2023]. **b**) Median symmetry score during training Color code is as in panel **a**. **c**) Same as in panel **a** for each layer in the model with and without symmetric initialization. Each layer is color-coded as in the illustration on the left. All plots show the median and the interquartile range across the heads of a given layer.